END

FILMED

DTIC

A FINITE ELEMENT COMPUTATION OF THE
ELECTROMAGNETIC FIELDS WITHIN AN
ENGINE INLET MODEL

THESIS

AFIT/GE/EE/82D-25   Thomas G. Cooper
                        1Lt   USAF

DTIC
ELECTE
FEB 2 2 1983

A

DEPARTMENT OF THE AIR FORCE
AIR UNIVERSITY (ATC)
AIR FORCE INSTITUTE OF TECHNOLOGY

Wright-Patterson Air Force Base, Ohio

83 02 022 134

A FINITE ELEMENT COMPUTATION OF THE
ELECTROMAGNETIC FIELDS WITHIN AN
ENGINE INLET MODEL

THESIS

AFIT/GE/EE/82D-25   Thomas G. Cooper
                           1Lt   USAF

DTIC
ELECTE
FEB 2 2 1983

A
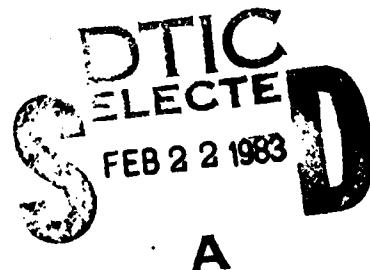
A FINITE ELEMENT COMPUTATION OF THE ELECTROMAGNETIC FIELDS WITHIN AN ENGINE INLET MODEL

THESIS

AFIT/GE/EE/82D   Thomas G. Cooper
                                  1Lt   USAF

A FINITE ELEMENT COMPUTATION OF

THE ELECTROMAGNETIC FIELDS WITHIN

AN ENGINE INLET MODEL

THESIS

Presented to the Faculty of The School of Engineering

of the Air Force Institute of Technology

Air University

in Partial Fulfillment of the

Requirements for the Degree of

Master of Science

by

Thomas G. Cooper

1st Lt   USAF

Graduate Electrical Engineering

December 1982

Approved for public release; distribution unlimited.

Acknowledgements

I wish to express appreciation to my faculty advisors Capt. Thomas W. Johnson, Capt. Pedro L. Rustan and Dr. John Jones for their willingness to provide assistance in this thesis project.

I want to especially thank my wife, Tampa, for her patience, understanding and encouragement during the last year and one half.

Table of Contents

List of Figures

Abstract

The method of coupled azimuthal potentials (CAP) was applied to a waveguide model of an axially symmetric engine inlet to analyze the fields in the region where the front face of the engine terminates the waveguide. Appropriate boundary conditions were derived and the finite element method was used to solve for the potentials.

The Lagrangian of the CAP equations does not provide for the enforcement of Neumann boundary conditions. This prevents exact implementation of the correct boundary conditions for the azimuthal magnetic field. Dirichlet boundary conditions for the azimuthal electric and magnetic fields were enforced for a standing wave condition in the inlet model with a conducting flat plate termination. The computed values for the interior field components were compared by evaluating the standard deviation. Three trials were performed with varying finite element mesh densities. It was found that as the mesh density increased, the standard deviation for the computed field components decreased. However, from an interpolation of the error measurements, it was determined that an extremely fine mesh is required for an acceptable error (approximately 7500 triangles/λ_o^2 for 2% error). For this reason the finite element implementation of the CAP equations for this jet engine inlet model is unfeasible.

A FINITE ELEMENT COMPUTATION OF THE
ELECTROMAGNETIC FIELDS WITHIN AN
ENGINE INLET MODEL

I. Introduction

Background

The jet engine inlet provides a significant contribution to the overall radar cross section of a modern aircraft. Before this contribution can be effectively reduced, the electromagnetic wave scattering phenomena from this region must be accurately evaluated and understood. This is a relatively difficult problem due to the generally complex nature of the geometry of the inlet. However, if an understanding of the scattering mechanisms from a simple intake geometry is developed, the insight could be analytically applied to the complex geometry of an actual inlet.

The engine intake usually consists of a hollow tubular structure terminatea by the fan blades of the engine compressor. It is well known that these fan blades significantly affect the radar return by modulating the echo (1:435). For this reason, any simplification in the geometry of an inlet model, would have to provide for the bladed structure of the compressor. The model to be used here will consist of a hollow circular cylindrical waveguide terminated by a conducting cone centered on a flat plate. Boundary conditions for the flat plate will be appropriately chosen to simulate the fan blade configuration.

Problem

The basic problem is to evaluate the electromagnetic wave interactions with a simplified termination model of a jet engine inlet.

Scope

This study will attempt to determine the scattered electromagnetic fields from a proposed intake termination model. No attempt will be made to recommend methods of reducing the radar cross section of a jet engine.

Literature Review

Several authors have previously developed and analyzed models of the jet engine intake area in an attempt to provide insight into the electromagnetic scattering.

John W. Moll and Rolf G. Seecamp analyzed an inlet modelled by a terminated circular cylindrical waveguide. The termination, which represents the initial stages of a compressor, consists of a pair of conducting planar blade structures as depicted in Figure 1. Each structure has a different number of blades and blade widths. The field incident on the opening of the inlet is represented by a sum of inwardly travelling TE modes. The backscattered field from the termination is expressed as a sum of TE modes travelling toward the opening of the duct. Any TM modes excited by the termination are neglected. Along the surface of the blades, the tangential electric field was set to zero. Using this boundary condition, a set of equations was obtained to solve for the scattering coefficients for the modes generated at the termination. The total field at the opening of the inlet is then equated to the sum of the incident and reflected modes. The Stratton-Chu integral is then applied to obtain the scattered field from any aspect angle (2).

A quite similar model was analyzed by P. H. Pathak and C. C. Huang. It consists of a hollow circular cylindrical waveguide terminated by a single pla: r blade ructure as in Figure 2. All of the blades are

2
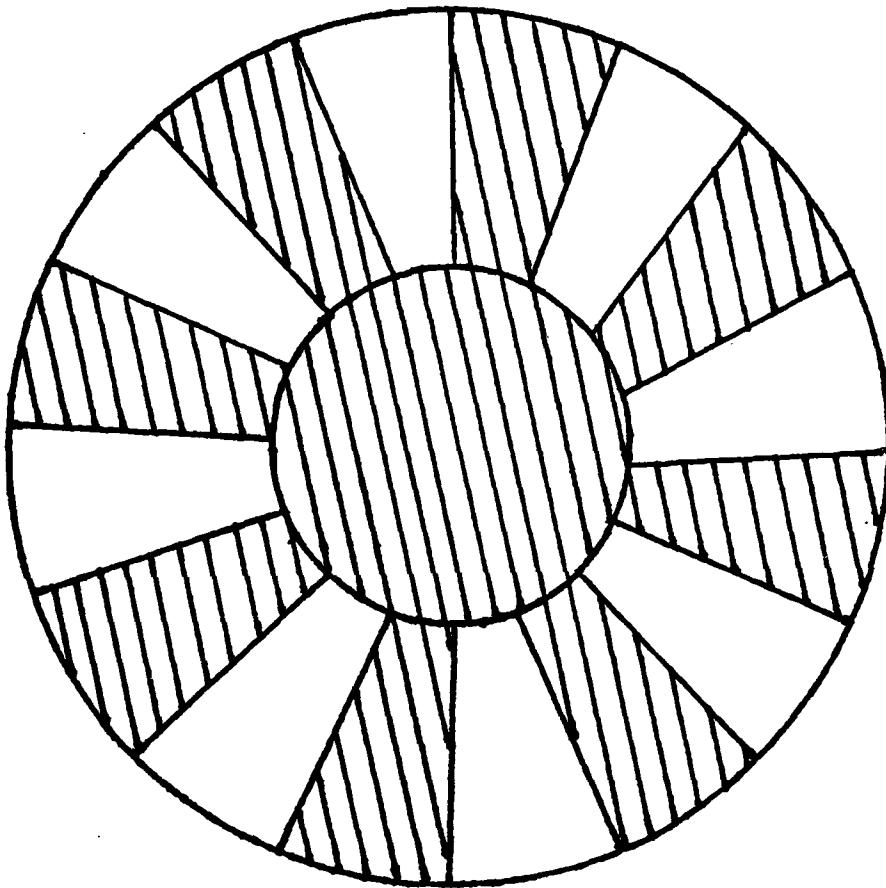
Figure 1. Form of Termination Used by Moll and Seecamp
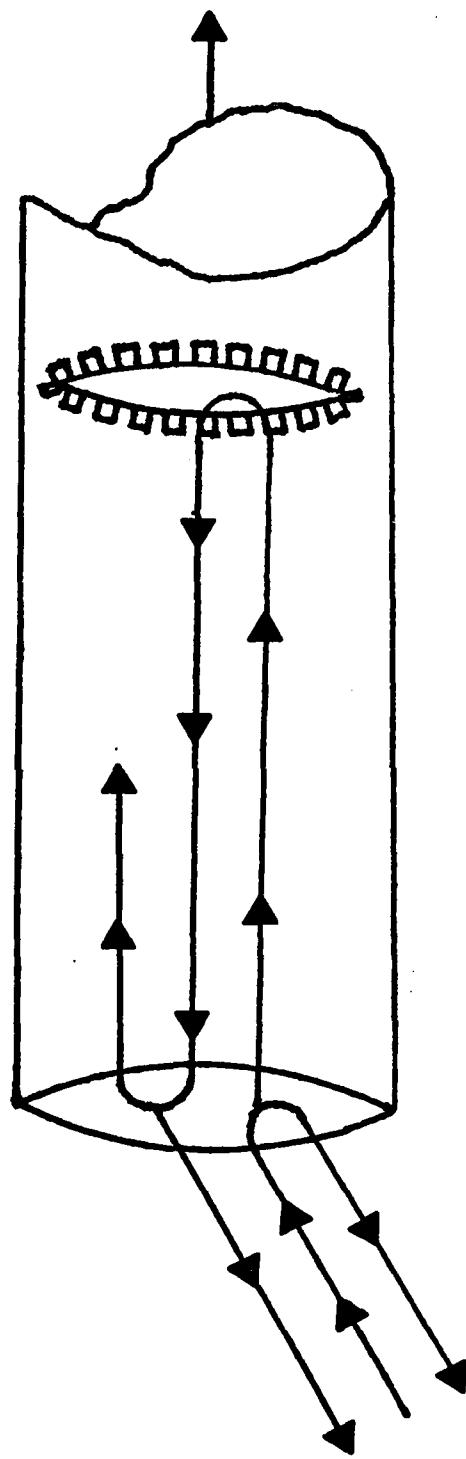
Figure 2. Inlet Model Used by Pathak and Huang

assumed to be of the same width separated by a finite angular distance. Basically their approach is to calculate scattering matrices at the opening of the duct (S_{11}, S_{12}, S_{22} and S_{21}) due to both an externally generated incident field and the reflected field due to the blade structure discontinuity. All of these matrices are calculated using the Uniform Theory of Diffraction. The scattering matrix at the termination is evaluated by a geometrical optics approximation to the current distribution ($J_B = 2 \cdot \hat{n} \times \overline{H}$) on the fan blades. The radar cross section of this model is then determined via the Multiple Scattering Method, which relates the backscattered field to the incident field (3).

T.W. Johnson and D. L. Moffatt analyzed the wave scattering from a circular cylindrical waveguide with a non-planar termination as illustrated in Figure 3. The termination considered is an axially symmetric cone centered on a flat plate. Both the cone and plate are perfectly conducting. Using the Wiener-Hopf technique, the scattering matrices for the opening of the waveguide are calculated. The dyadic magnetic Green's function and the Method of Moments are then used to numerically compute the current distribution on the cone. From this distribution, the reflection coefficient for the cone was determined for the TE_{11} mode. The radar cross section is then evaluated using this backscatter coefficient and the scattering matrices calculated for the open end of the waveguide (4).

Approach

The inlet model that will be analyzed represents a slight modification of the model used by Johnson and Moffat. It consists of a circular cylindrical waveguide terminated by a perfectly conducting cone centered on a flat plate. However, the boundary conditions enforced on the plate
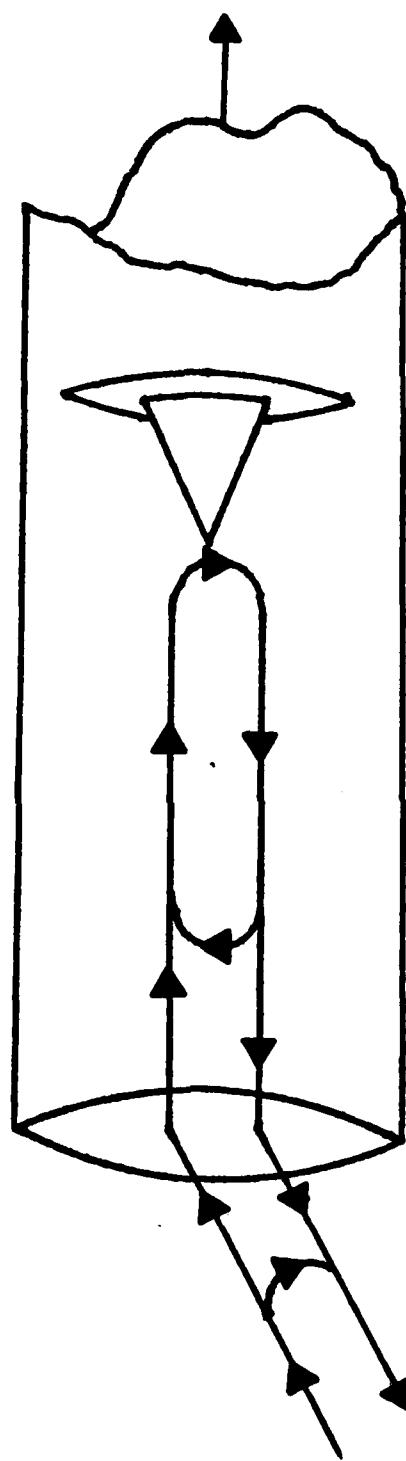
Figure 3. Non-planar Termination Used by Johnson and Moffat

6

will not be those of a perfect conductor. Instead, a set of boundary conditions will be used to make the flat plate resemble the blade structure of the compressor termination in an actual inlet.

Since fan blades are separated by a finite angular distance, any current induced on the blades cannot flow azimuthally. To simulate this effect in the model, the radially directed tangential magnetic field at the surface of the flat plate will be set to zero. This will eliminate azimuthal current in the plate and make it appear as a set of infinitely thin wires directed radially outward. The radially directed tangential electric field at the surface of the plate will also be set to zero, which is the appropriate boundary condition for a conductor.

With the aid of the Coupled Azimuthal Potential (CAP) formulation, the finite element method and the unimoment method, the total fields within the model will be determined. The CAP consists of two second order differential equations developed by Morgan, Chang and Mei to solve scattering problems involving generally lossy isotropic inhomogenous rotationally symmetric media (5). These potentials, which are directly related to the electric and magnetic fields, will be numerically computed using the finite element method. This requires that an integral functional be used to set up the numerical solution for the fields in the waveguide. The functional, when minimized, is analytically equivalent to enforcing the differential equations. Finally, the unimoment method will be used to determine a linear combination of fields which will satisfy the boundary conditions of the inlet model.

Chapter II will be devoted to presenting the CAP formulation theory and the finite element implementation of the differential equations. In addition, the application of the unimoment method to this problem will be detailed.

7

Chapter III will give the results and Chapter IV the conclusions
and recommendations resulting from the analysis of the inlet model.

II. Analytical Formulation

This chapter will discuss the analysis used in obtaining the system of equations for evaluation of the electromagnetic fields in the interior of the engine inlet model. The derivation of the coupled azimuthal potential (CAP) formulation will be presented. Numerical computation of the CAP by use of the finite element method will also be developed. In addition, the application of the unimoment method to calculate the total fields will be discussed.

CAP Formulation

The CAP is valid in generally inhomogenous isotropic rotationally symmetric media (bodies of revolution) as shown in Figure 4. Its basic utility is that it converts a three-dimensional scattering problem into one involving only two dimensions. Since the medium is axi-symmetric, the fields have a known functional behavior with respect to the ϕ coordinate (in a standard cylindrical coordinate system). Therefore, if the fields are determined for a constant R-Z cross section, they are known everywhere in the media.
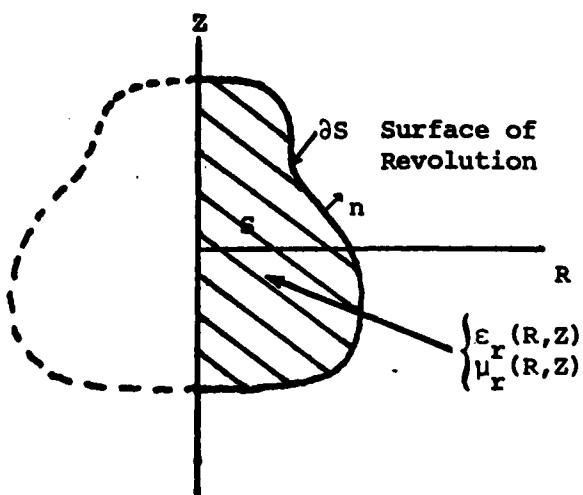
Figure 4. Meridional Two-dimensional Solution Domain (6:203)

9

The CAP formulation development begins by defining a Cartesian coordinate system consisting of normalized circular cylindrical coordinates. All points within the system may be given by (R, Z, ϕ) where $R = K_o \rho$, $Z = K_o z$, $\phi = \phi$ and $K_o = 2\pi/\lambda_o$ is the free space wave number of the fields. The fields are then expanded into an exponential Fourier series in the ϕ coordinate:

$$\overline{E}(R, Z, \phi) = \sum_{n=-\infty}^{\infty} \overline{e}_n(R, Z) \exp(jn\phi) \tag{1}$$

$$\eta_o \overline{H}(R, Z, \phi) = \sum_{n=-\infty}^{\infty} \overline{h}_n(R, Z) \exp(jn\phi) \tag{2}$$

where $\eta_o = \mu_o/\varepsilon_o$. When these expansions are placed in Maxwell's equations, $\nabla \times \overline{E} = -j\omega\mu\overline{H}$ and $\nabla \times \overline{H} = j\omega\varepsilon\overline{E}$, the following coupled system of equations is obtained:

$$\varepsilon_r e_{\phi,n} = j \left[\frac{\partial h_{Z,n}}{\partial R} - \frac{\partial h_{R,n}}{\partial Z} \right] \tag{3}$$

$$\mu_r h_{\phi,n} = j \left[\frac{\partial e_{R,n}}{\partial Z} - \frac{\partial e_{Z,n}}{\partial R} \right] \tag{4}$$

$$R\varepsilon_r e_{R,n} = j \left[\frac{\partial (Rh_{\phi,n})}{\partial Z} - jnh_{Z,n} \right] \tag{5}$$

$$R\mu_r h_{R,n} = j \left[jne_{Z,n} - \frac{\partial (Re_{\phi,n})}{\partial Z} \right] \tag{6}$$

$$R\varepsilon_r e_{Z,n} = j \left[jnh_{R,n} - \frac{\partial (Rh_{\phi,n})}{\partial R} \right] \tag{7}$$

$$R\mu_r h_{Z,n} = j \left[\frac{\partial (Re_{\phi,n})}{\partial R} - jne_{R,n} \right] \tag{8}$$

Substituting among those equations, it can easily be shown that

10

$$\bar{e}_n(R,Z) = jf_n(n\nabla\psi_1 + R\mu_r\hat{\phi} \times \nabla\psi_2) + \hat{\phi}(\psi_1/R) \qquad (9)$$

$$\bar{h}_n(R,Z) = jf_n(n\nabla\psi_2 - R\epsilon_r\hat{\phi} \times \nabla\psi_1) + \hat{\phi}(\psi_2/R) \qquad (10)$$

where $\psi_1/R = e_{\phi,n}$, $\psi_2/R = h_{\phi,n}$ and the gradient operator, ∇, is defined as $\hat{R}\ \partial/\partial R + \hat{Z}\ \partial/\partial Z$. Additionally,

$$f_n(R,Z) = \mu_r(R,Z)\ \epsilon_r(R,Z)R^2 - n^2 \qquad (11)$$

From Eqs (9) and (10) the radial and Z directed components of the electric and magnetic field may be determined. These components may be shown to be

$$e_R(R,Z) = jf_n(\frac{\partial Re_\phi}{\partial Z} - R\ \frac{\partial Rh_\phi}{\partial R}) \qquad (12)$$

$$e_Z(R,Z) = jf_n(- \frac{\partial Re_\phi}{\partial R} - R\ \frac{\partial Rh_\phi}{\partial Z}) \qquad (13)$$

$$h_R(R,Z) = jf_n(R\ \frac{\partial Rh_\phi}{\partial Z} - \frac{\partial Rh_\phi}{\partial R}) \qquad (14)$$

$$h_Z(R,Z) = jf_n(\frac{\partial Rh_\phi}{\partial Z} + R\ \frac{\partial Re_\phi}{\partial R}) \qquad (15)$$

The coupled potentials, ψ_1 and ψ_2, satisfy a system of partial differential equations given by:

$$\nabla\ f_n(R\epsilon_r\nabla\psi_1 + n\hat{\phi} \times \nabla\psi_2)\ + \epsilon_r\ \psi_1/R = 0$$

$$\nabla\ f_n(R\mu_r\nabla\psi_2 - n\hat{\phi} \times \nabla\psi_1)\ + \mu_r\ \psi_2/R = 0$$

To utilize the finite element method to numerically compute the potentials, it is necessary to develop a Lagrangian functional. The stationary point of the integral of this functional is analytically equivalent to the partial differential equations. For this set of differential equations

11

$$L = f_n \quad \nabla\psi_1 (R\epsilon_r \nabla\psi_1 + n\hat{\phi} \times \nabla\psi_2) +$$

$$\nabla\psi_2 \cdot (R\mu_r \nabla\psi_2 - n\hat{\phi} \times \nabla\psi_1) - (\epsilon_r\psi_1^2 + \mu_r\psi_2^2)/R \quad (14)$$

Finite Element Method

The finite element method is a numerical method of calculating the approximate solution of a partial differential equation in an enclosed area. It does so by assuming a form of the solution (linear, quadratic, etc.) within a set of "finite elements" which span the total area. By integrating an integral functional over each element, the displacement of a single nodal value on an element is related to adjacent nodal values. This process results in a system of equations. The simultaneous solution of this set of equations results in the values of nodal coefficients, thus providing a piecewise approximation of the solution from node to node.

When utilizing the Lagrangian, the term $(\epsilon_r\psi_1^2 + \mu_r\psi_2^2)/R$ produces a singularity along the $R = 0$ axis. To overcome this difficulty, a change of variable must be performed on the scalar potentials, letting $Re_{\phi,n} = \psi_1$ and $Rh_{\phi,n} = \psi_2$. It then becomes necessary that the boundary conditions satisfied by the azimuthal field quantities along $R = 0$ be specified. These boundary conditions are:

$$e_{\phi,n}(R,Z) \Big|_{R=0} = h_{\phi,n}(R,Z) \Big|_{R=0} = 0 \quad \text{for } n^2 \neq 1 \quad (15)$$

$$3\frac{\partial e_{\phi,n}}{\partial R} + (\frac{\partial \ln\epsilon_r}{\partial R}) e_{\phi,n} \Big|_{R=0} = 0 \quad \text{for } n^2 = 1 \quad (16)$$

$$3\frac{\partial h_{\phi,n}}{\partial R} + (\frac{\partial \ln\mu_r}{\partial R}) h_{\phi,n} \Big|_{R=0} = 0 \quad \text{for } n^2 = 1 \quad (17)$$

12

The boundary conditions for $n^2 = 1$ reduce to homogenous Neumann boundary conditions when the relative permittivity and permeability are invariant with respect to R (5:416). To enforce these conditions all that is required is to allow the nodal values to "float".

For the engine inlet problem, the cross section of the model is subdivided into a finite number of triangular elements. A typical section is illustrated in Figure 5. The assumption is made that the scalar azimuthal potentials vary linearly over each of the elements. This necessitates the use of linear basis functions defined on each node of every element.
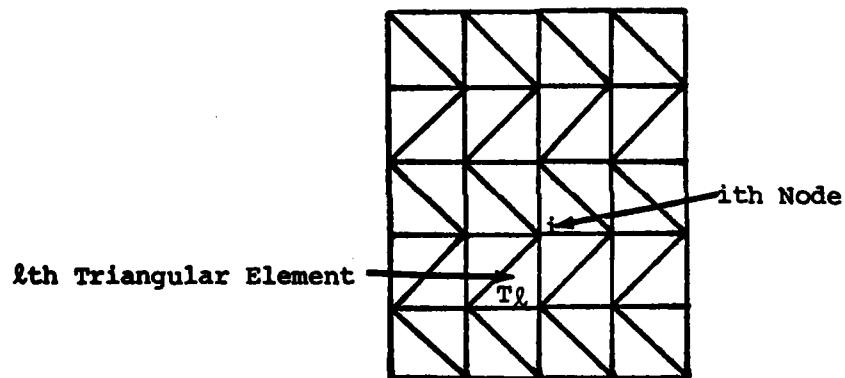
Figure 5. Typical Finite Element Section of Model Cross Section

These pyramidal functions will have a value of unity on a specified node and a value of zero on neighboring nodes. For the ith node on the ℓth element, the linear basis function, $\phi_i(R,Z)$, is defined as

$$\phi_i(R,Z) = a_{i,\ell} + b_{i,\ell} R + c_{i,\ell} Z \qquad (18)$$

The real constants $a_{i,\ell}$, $b_{i,\ell}$, and $c_{i,\ell}$ for $i = 1,2,3$ on each element may be evaluated by means of the following equations:

13

$$a_{1,\ell} = \frac{Z_{2,\ell} \, R_{3,\ell} - R_{2,\ell} \, Z_{3,\ell}}{\Delta_\ell} \tag{19}$$

$$b_{1,\ell} = \frac{Z_{3,\ell} - Z_{2,\ell}}{\Delta_\ell} \tag{20}$$

$$c_{1,\ell} = \frac{R_{2,\ell} - R_{3,\ell}}{\Delta_\ell} \tag{21}$$

$$a_{2,\ell} = \frac{Z_{3,\ell} \, R_{1,\ell} - R_{3,\ell} \, Z_{1,\ell}}{\Delta_\ell} \tag{22}$$

$$b_{2,\ell} = \frac{Z_{1,\ell} - Z_{3,\ell}}{\Delta_\ell} \tag{23}$$

$$c_{2,\ell} = \frac{R_{3,\ell} - R_{1,\ell}}{\Delta_\ell} \tag{24}$$

$$a_{3,\ell} = \frac{Z_{1,\ell} \, R_{2,\ell} - R_{1,\ell} \, Z_{2,\ell}}{\Delta_\ell} \tag{25}$$

$$b_{3,\ell} = \frac{Z_{2,\ell} - Z_{1,\ell}}{\Delta_\ell} \tag{26}$$

$$c_{3,\ell} = \frac{R_{1,\ell} - R_{2,\ell}}{\Delta_\ell} \tag{27}$$

where
$$\Delta_\ell = \begin{vmatrix} 1 & R_{1,\ell} & Z_{1,\ell} \\ 1 & R_{2,\ell} & Z_{2,\ell} \\ 1 & R_{3,\ell} & Z_{3,\ell} \end{vmatrix} \tag{28}$$

and is twice the area of a triangle (7:547). These computations assume a clockwise ordering of the node numbers on each element.

The azimuthal field components within the inlet model may now be expressed as

$$\hat{\phi} \cdot \overline{e}_n(R,Z) = \sum_{i=1}^{N} \alpha_i \phi_i(R,Z) \tag{29}$$

14

and
$$\hat{\phi} \cdot \overline{h}_n(R,Z) = \sum_{i=1}^{N} \beta_i \phi_i(R,Z). \qquad (30)$$

The complex nodal values of $e_{\phi,n}$ and $h_{\phi,n}$ at a particular node, i, are represented by α_i and β_i respectively (6:204).

The finite element approach begins with the substitution of the azimuthal field expansions in Eqs (29) and (30) into the integral functional

$$F = \int_s L(R,Z,\psi_1,\psi_2,\nabla\psi_1,\nabla\psi_2)\,dRdZ \qquad (31)$$

where $L(R,Z,\psi_1,\psi_2,\nabla\psi_1,\nabla\psi_2)$ is defined by Eq (14). This results in

$$F = \int_s f_n \quad \nabla(R\sum_{i=1}^{N}\gamma_i\phi_i) \cdot \quad Re_r \ \nabla(R\sum_{i=1}^{N}\gamma_i\phi_i) \ +$$

$$n \hat{\phi} \times \nabla \ (R\sum_{i=1}^{N}\beta_i\phi_i) \quad + \nabla(R\sum_{i=1}^{N}\beta_i\phi_i) \ \cdot$$

$$R\mu_r \ \nabla(R\sum_{i=1}^{N}\beta_i\phi_i) - n \hat{\phi} \times \nabla(R\sum_{i=1}^{N}\gamma_i\phi_i) \quad -$$

$$\varepsilon_r \ R(\sum_{i=1}^{N}\gamma_i\phi_i)^2 - \mu_r \ R \ (\sum_{i=1}^{N}\beta_i\phi_i)^2 \ dRdZ \qquad (32)$$

The stationary point of F is obtained by differentiating the functional with respect to each of the nodal coefficients and setting it equal to zero.

$$\frac{\partial F}{\partial \gamma_m} = 0$$

$$= \int_s f_n \quad (R\sum_{i=1}^{N}\gamma_i\phi_i) \ \cdot \ (Re_r \ \nabla(R\phi_m)) + \nabla(R\phi_m) \ \cdot$$

$$(Re_r \ \nabla(R\sum_{i=1}^{N}\gamma_i\phi_i) + n \hat{\phi} \times \nabla(R\sum_{i=1}^{N}\beta i\phi i)) + \nabla(R\sum_{i=1}^{N}\beta i\phi i) \ \cdot$$

15

$$(-n \, \hat{\phi} \times \nabla(R\phi_m)) \quad - 2\epsilon_r \, R \, \sum_{i=1}^{I} \gamma_i \phi_i \phi_m \, dRdZ$$

$$= \sum_{i=1}^{N} \gamma_i \int_s f_n \quad \nabla(R\phi_i) \cdot (R\epsilon_r \, \nabla(R\phi_m)) + \nabla(R\phi_m) \cdot$$

$$(R\epsilon_r \, \nabla(R\phi_i)) \quad - 2\epsilon_r \, R\phi_i \phi_m \, dRdZ$$

$$+ \sum_{i=1}^{N} \beta_i \int_s f_n \quad \nabla(R\phi_m) \cdot n \, \hat{\phi} \times \nabla(R\phi_i) + \nabla(R\phi_i) \cdot$$

$$(-n \, \hat{\phi} \times \nabla(R\phi_m)) \quad dRdZ$$

$$= \sum_{i=1}^{N} \gamma_i \int_s 2f_n \, R\epsilon_r \, \nabla(R\phi_i) \cdot \nabla(R\phi_m) - 2\epsilon_r \, R\phi_i \phi_m \, dRdZ$$

$$+ \sum_{i=1}^{N} \beta_i \int_s 2f_n \, (\nabla \, (R\phi_m) \cdot n \, \hat{\phi} \times \nabla(R\phi_i)) \, dRdZ$$

Therefore

$$\sum_{i=1}^{N} \gamma_i \int_s f_n \, R\epsilon_r \, \nabla(R\phi_i) \cdot \nabla(R\phi_m) - \epsilon_r \, R \, \phi_i \phi_m \, dRdZ$$

$$+ \sum_{i=1}^{N} \beta_i \int_s nf_n \, \nabla(R\phi_m) \cdot \hat{\phi} \times \nabla(R\phi_i) \, dRdZ = 0 \qquad (33)$$

for $m = 1, 2, \ldots, N$.

$$\frac{\partial F}{\partial \beta_m} = 0$$

$$= \int_s f_n \quad \nabla(R \sum_{i=1}^{N} \gamma_i \phi_i) \cdot n \, \hat{\phi} \times \nabla(R\phi_m) + \nabla(R \sum_{i=1}^{N} \beta_i \phi_i) \cdot$$

$$R\mu_r \, \nabla(R\phi_m) + \nabla(R\phi_m) \cdot (R\mu_r \, \nabla(R \sum_{i=1}^{N} \beta_i \phi_i) -$$

16

$$n \, \hat{\phi} \times \nabla(R \sum_{i=1}^{N} \gamma_i \phi_i)) \quad - 2\mu_r \, R \sum_{i=1}^{N} \beta_i \phi_i \phi_m \; dRdZ$$

$$= \sum_{i=1}^{N} \beta_i \int_s f_n \quad \nabla(R\phi_i) \cdot (R\mu_r \, \nabla(R\phi_m)) + \nabla(R\phi_m) \cdot (R\mu_r \, \nabla(R\phi_i))$$

$$- 2\mu_r R\phi_i \phi_m \; dRdZ$$

$$+ \sum_{i=1}^{N} \gamma_i \int_s f_n \quad \nabla(R\phi_i) \cdot n \, \hat{\phi} \times \nabla(R\phi_m) - \nabla(R\phi_m) \cdot n \, \hat{\phi} \times \nabla(R\phi_i) \quad dRdZ$$

$$= \sum_{i=1}^{N} \beta_i \int_s 2f_n \; R\mu_r \, \nabla(R\phi_i) \cdot \nabla(R\phi_m) - 2\mu_r \, R\phi_i \phi_m \; dRdZ$$

$$- \sum_{i=1}^{N} \gamma_i \quad_s 2f_n \; R \, \nabla(R\phi_m) \cdot n \, \hat{\phi} \times \nabla(R\phi_i) \; dRdZ.$$

Therefore,

$$\sum_{i=1}^{N} \beta_i \int_s f_n R\mu_r \, \nabla(R\phi_i) \cdot \nabla(R\phi_m) - \mu_r \, R\phi_i \phi_m \; dRdZ$$

$$- \sum_{i=1}^{N} \gamma_i \int_s n f_n \; R \, \nabla(R\phi_m) \cdot \hat{\phi} \times \nabla(R\phi_i) \; dRdZ = 0 \qquad (34)$$

for m = 1,2, ..., N. For the inlet, only the case for n=1 will be examined. In addition, it will be assumed that $\mu_r = \epsilon_r = 1$. Equations (33) and (34) then become

$$\sum_{i=1}^{N} \gamma_i \int_s f_1 \; R \, \nabla(R\phi_i) \cdot \nabla(R\phi_m) - R\phi_i \phi_m \; dRdZ$$

$$+ \sum_{i=1}^{N} \beta_i \int_s f_1 \; \nabla(R\phi_m) \cdot \hat{\phi} \times \nabla(R\phi_i) \; dRdZ = 0 \qquad (35)$$

17

$$\sum_{i=1}^{N} \beta_i \int_S f_1 \, R \, \nabla(R\phi_i) \cdot \nabla(R\phi_m) - R\phi_i\phi_m \, dRdZ$$

$$- \sum_{i=1}^{N} \gamma_i \int_S f_1 \, \nabla(R\phi_m) \cdot \hat{\phi} \times \nabla(R\phi_i) \, dRdZ = 0 \qquad (36)$$

Equations (35) and (36) are integrated only over the elements connected to node m and relate γ_m and β_m to adjacent nodal values of γ_i and β_i. For the mesh illustrated in Figure 5, 14 adjacent nodal values will be related to one another. These equations will produce a 2N x 2N sparse, banded symmetric matrix, which is characteristic of any finite element computations.

All integrals to be evaluated in Eqs (35) and (36) are of the general form

$$P_{rs} = \int_S R^r Z^s \, dRdZ \qquad (37)$$

$$Q_{rs} = \int_S \frac{R^r Z^s}{R^2-1} \, dRdZ \qquad (38)$$

A simple method for computing both types of these integrals exists by invoking the two-dimensional Stoke's theorem and converting the surface integrals into line integrals. The general formula is given by

$$\int_S g(R) Z^s \, dRdZ = \frac{1}{s+1} \oint_C g(R) Z^{s+1}(R) \, dR \qquad (39)$$

where the integration is performed in a clockwise manner around the triangular elements. The factor $g(R)$ is any arbitrary function of R (6:205). If Z is expanded in terms of R i.e. $Z = mR + b$ where m = slope and b = Z intercept, the form of Q_{rs} is

18

$$\int_{R_i}^{R_j} \frac{R^n}{R^2-1} \, dR \qquad (40)$$

where n ranges from 0 to r+s+1 (6:205). These segmented integrations will produce complex values as the integration passes through $R^2 = 1$. If $n = 0$

$$\int_{R_i}^{R_j} \frac{1}{R^2-1} \, dR = \int_{R_i}^{R_j} \frac{.5}{R-1} \, dR - \int_{R_i}^{R_j} \frac{.5}{R+1} \, dR$$

$$= \lim_{\varepsilon \to 0} \int_{R_i}^{1-\varepsilon} \frac{.5}{R-1} \, dR + \int_{1+\varepsilon}^{R_j} \frac{.5}{R-1} \, dR - \int_{R_i}^{R_j} \frac{.5}{R+1} \, dR$$

$$= \lim_{\varepsilon \to 0} \; .5\ln(R-1) \Big|_{R_i}^{1-\varepsilon} + .5\ln(R-1) \Big|_{1+\varepsilon}^{R_j} - .5\ln(R+1) \Big|_{R_i}^{R_j}$$

$$= \lim_{\varepsilon \to 0} \; .5\ln(-\varepsilon) - .5\ln(R_i-1) + .5\ln(R_j-1) - .5\ln(\varepsilon)$$

$$-.5\ln(R_j+1) + .5\ln(R_i+1)$$

$$= \lim_{\varepsilon \to 0} \; .5 \, n(\varepsilon) \pm \frac{\pi}{2} i - .5\ln(R_i-1) + .5\ln(R_j-1)$$

$$- .5\ln(\varepsilon) - .5\ln(R_j+1) + .5\ln(R_i+1)$$

$$= .5\ln \left(\frac{(R_j-1)(R_i+1)}{(R_i-1)(R_j+1)} \right) \pm \frac{\pi}{2} i \qquad (41)$$

A similar development for n=1 yields

19

$$\int_{R_i}^{R_j} \frac{R}{R^2-1} \, dR = .5\ln\left(\frac{(R_j-1)(R_j+1)}{(R_i-1)(R_i+1)}\right) \pm \frac{\Pi}{2} i \qquad (42)$$

Higher order integrals of this form may be generated by the recursion formula

$$\int_{R_i}^{R_j} \frac{R^n}{R^2-1} \, dR = \int_{R_i}^{R_j} \frac{R^{n-2}}{R^2-1} \, dR + \frac{R_j^{n-1} - R_i^{n-1}}{n-1} \qquad (43)$$

(6:205).

In general, the homogenous system of linear equations defined by (35) and (36) does not have a unique solution. However, some values of nodal coefficients along the exterior boundaries of the inlet model will be specified as Dirichlet boundary conditions. These boundary conditions can be used to render a unique solution to the system of equations. Before the enforcement of boundary conditions, the form of the linear system is

$$\begin{vmatrix} K_{1,1} & K_{1,2} & K_{1,3} & \cdots & K_{1,2N} \\ K_{2,1} & K_{2,2} & K_{2,3} & \cdots & K_{2,2N} \\ K_{3,1} & K_{3,2} & K_{3,3} & \cdots & K_{3,2N} \\ \vdots & \vdots & \vdots & \vdots & \vdots \\ K_{2N,1} & K_{2N,2} & K_{2N,3} & \cdots & K_{2N,2N} \end{vmatrix} \begin{vmatrix} \gamma_1 \\ \beta_1 \\ \gamma_2 \\ \vdots \\ \beta_N \end{vmatrix} = \begin{vmatrix} 0 \\ 0 \\ 0 \\ \vdots \\ 0 \end{vmatrix} \qquad (44)$$

where the K's are generated by integration of the Lagrangian over the elements and the γ's and β's are the values of the nodal coefficients. Now if, for example, β_1 is specified as a Dirichlet boundary condition, and has a value of V_1, the system may be modified to

20

$$
\begin{vmatrix}
K_{1,1} & 0 & K_{1,3} & \cdots & K_{1,2N} \\
0 & 1 & 0 & \cdots & 0 \\
K_{3,1} & 0 & K_{3,1} & \cdots & K_{3,2N} \\
\vdots & \vdots & \vdots & \vdots & \vdots \\
K_{2N,1} & 0 & K_{2N,3} & \cdots & K_{2N,2N}
\end{vmatrix}
\begin{vmatrix}
\gamma_1 \\ \beta_1 \\ \gamma_2 \\ \vdots \\ \beta_N
\end{vmatrix}
=
\begin{vmatrix}
-K_{12}\,V_1 \\ V_1 \\ -K_{3,2}\,V_1 \\ \vdots \\ -K_{2N,2}\,V_1
\end{vmatrix}
\qquad (45)
$$

This process is performed for all Dirichlet boundary conditions allowing a unique solution to be obtained (8:52).

Unimoment Method

The finite element method, in conjunction with the CAP formulation, can be used to numerically compute a single set of electromagnetic fields for given Dirichlet boundary conditions. However, h_ϕ requires that certain Neumann boundary conditions be met. The unimoment method can be used to determine a combination of solutions that will satisfy these Neumann conditions.

Boundary Condition Formulations. The solution domain for the engine inlet model is shown in Figure 6. The included angles α and δ give the slanting angle of the axisymmetric cone and the elevation angle of the back plate, respectively. All relations derived in this section follow from Eqs (3) through (8) directly.

21
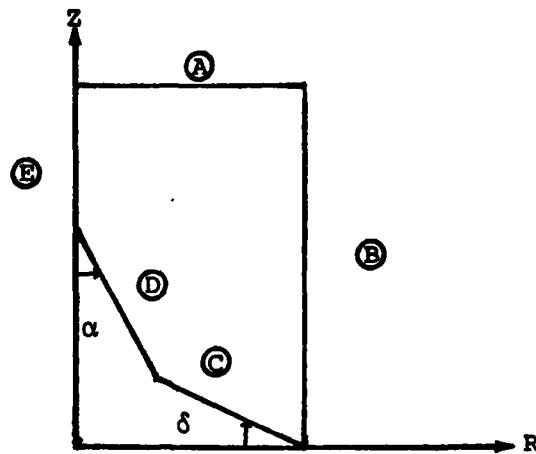
Figure 6. Solution Domain for Engine Inlet Model

Boundary Ⓐ represents the opening of the inlet model. Along this segment, Dirichlet conditions for the fields incident on the mouth of the duct are specified. Due to the cylindrical nature of this problem, these conditions are in terms of the Bessel functions J_n' (K_cR) for e_ϕ and $J_n(K_cR)$ for h_ϕ.

The outer wall of the waveguide is labelled Ⓑ. Because of the perfectly conducting nature of this surface, the tangential components of the electric field, e_z and e_ϕ, must be identically zero. In terms of azimuthal field quantities only, the equivalent boundary conditions are

$$e_\phi = 0 \tag{46}$$

and
$$\nabla(\psi_2) \cdot \hat{n} = \frac{\partial(Rh_\phi)}{\partial R} = 0. \tag{47}$$

The bladed structure of the fans in the initial stages of a compressor, is approximated by the back plate, Ⓒ. As stated earlier, azimuthal current flow on the face of this plate is to be eliminated. This requires enforcement of the boundary condition

22

$$h_R \cos \delta - h_Z \sin \delta = 0 \tag{48}$$

or equivalently

$$\left(\frac{\partial Rh\phi}{\partial R} - R \frac{\partial Re\phi}{\partial Z}\right) \cos \delta = \left(\frac{\partial Rh\phi}{\partial Z} + R \frac{\partial Re\phi}{\partial Z}\right) \sin \delta. \tag{49}$$

Additionally, it is required that

$$e_R \cos \delta = e_Z \sin \delta = 0 \tag{50}$$

which implies

$$\left(\frac{\partial Re\phi}{\partial Z} - R \frac{\partial Rh\phi}{\partial R}\right) \sin \delta = \left(- \frac{\partial Re\phi}{\partial R} - R \frac{\partial Rh\phi}{\partial Z}\right) \cos \delta \tag{51}$$

Since the cone, ⓓ , like the wall of the waveguide, ⓑ , is perfectly conducting, it has similar boundary conditions. These conditions may be expressed as:

$$e_\phi = 0 \tag{52}$$

and

$$\left(\frac{\partial Re\phi}{\partial Z} - R \frac{\partial Rh\phi}{\partial R}\right) \cos = \left(- \frac{\partial Re\phi}{\partial R} - R \frac{\partial Rh\phi}{\partial Z}\right) \sin \tag{53}$$

for $0 < \alpha < \pi$. At $\alpha = 0$ and $\alpha = \pi$ the boundary conditions are identical to those for ⓔ which are given by Eqs (15), (16), and (17).

Unimoment Method Formulation. The general process of applying the unimoment method, consists of several steps. First, a form of the field variations is assumed along each exterior boundary of the inlet model. Then, using these Dirichlet boundary conditions, the resulting interior fields are computed using the finite element implementation of the CAP equations. This process is repeated N times for N different forms of the field variations. From these N solutions a set of weighting functions are calatulated to enforce the Neumann boundary conditions in the mean sense.

23

As an example, consider the boundary conditions along the exterior wall of the circular cylindrical waveguide given by

$$e_\phi = 0 \tag{54}$$

and

$$\frac{\partial Rh_\phi}{\partial R} = 0 \tag{55}$$

Assume that h_ϕ varies as $\sin \frac{n\pi Z}{Z_0}$ along this surface, for $n = 1, 2, \ldots, N$ where N is the total number of nodes along the boundaries of the model. Appropriate field variations along the other boundaries must be also enforced simultaneously with this one. For each n a solution is obtained, thus specifying γ_i, β_i, a_i, b_i and c_i for each node. For the total field solution, which is a linear combination of each of the n solutions, it is required that

$$\sum_{n=1}^{N} W_n \frac{\partial Rh_{\phi n}}{\partial R} = 0 \tag{56}$$

along the wall of the waveguide. The W_n's are the weighting functions for the nth solution. These equations are than enforced using testing functions such that

$$\sum_{n=1}^{N} W_n \int_{0}^{Z_0} \left(\frac{\partial Rh_{\phi n}}{\partial R}\right) \sin \frac{n\pi Z}{Z_0} dZ = 0 \tag{57}$$

and consequently enforce the Neumann boundary condition in the mean sense. These equations will generate a $N \times N$ matrix, and produce a linear system of equations

$$\underline{B}\ \underline{W} = 0 \tag{58}$$

24

To produce a unique solution, the right hand side of the equation must be non-zero. For this reason some small δ must be used, $\delta << 1$, so that

$$\underline{B}\ \underline{W} = \underline{\delta} \qquad . \qquad (59)$$

This is the general method to be used to enforce Neumann boundary conditions.

III.   Results

The results presented in this section concern only the validation of the software developed for the finite element implementation of the coupled azimuthal potential differential equations. Appendix A contains a listing of the program used for this procedure. In addition, a description of all variables used in the program is given in this appendix.

To insure the program was correctly computing the azimuthal field components, it was necessary to enforce boundary conditions for a known wave solution. For this reason, boundary conditions for a standing wave in a circular cylindrical waveguide·terminated by a flat conducting plate were used. This required a minor modification of the inlet model. The angles α and δ, defined in Figure 6, were set to zero and conducting boundary conditions established along the back plate. As stated earlier the boundary conditions for a conductor are

$$e_\phi = 0 \tag{60}$$

and

$$\nabla(Rh_\phi) \cdot \hat{n} = 0 \tag{61}$$

Since it is not possible to directly enforce the Neumann condition given by Equation (61) with the minimized Lagrangian functional, the Dirchlet boundary conditions for a standing wave were applied along all conducting surfaces.

For a standing wave in a circular cylindrical waveguide, the electric and magnetic fields must satisfy the following set of equations:

$$H_z = A J_1(j_{11}' \rho/a) \sin K_z z \, e^{j\phi} \tag{62}$$

$$E_\rho = -\frac{1}{K_c^2} \frac{j\omega\mu}{\rho} \frac{\partial H_z}{\partial \phi} \tag{63}$$

$$E_\phi = \frac{1}{K_c^2} j\omega\mu \; \frac{\partial H_z}{\partial \rho} \qquad (64)$$

$$H_\rho = \frac{1}{K_c^2} \frac{\partial^2 H_z}{\partial \rho \partial z} \qquad (65)$$

and
$$H_\phi = \frac{1}{K_c^2} \frac{1}{\rho} \frac{\partial^2 H_z}{\partial \phi \partial z} \quad (9{:}415) \qquad (66)$$

Only azimuthal field quantities are being calculated, so it is only neces-
sary to determine the forms of E_ϕ and H_ϕ. Using the above relations it
is easily shown that

$$E_\phi = \frac{A}{K_c} j\omega\mu \; J_1' \; (j_{11}' \; \rho/a) \; \sin K_z z \; e^{j\phi} \qquad (67)$$

$$H_\phi = \frac{A}{K_c^2} \frac{1}{\rho} K_z \; J_1 \; (j_{11}' \; \rho/a) \; \cos K_z z \; e^{j\phi} \qquad (68)$$

For all computations, the azimuthal dependence is suppressed and A is
assumed to be one.

As a first test case, a section of waveguide was evaluated with a
radius of $.5\lambda_o$ and a length of $1.5\lambda_o$. The finite element division con-
sisted of 96 triangles with 65 nodes. This resulted in a triangular
mesh density of 126 triangles per λ_o^2. Plots of the on-axis results
for the magnitude and phase of e_ϕ and h_ϕ are presented in Figures 7, 8,
9, and 10. In general, as is quite evident, the results are not promis-
ing. As a measure of the error, the square root of the average squared
error, i.e. $\sqrt{\Sigma(x-\hat{x})^2/N}$, was evaluated for the magnitudes of both
azimuthal field quantities. This resulted in a value of .462 for e_ϕ and
.524 for h_ϕ (all values were normalized to one).

It is believed the results from this first trial are so poor because
the triangular mesh was not sufficiently dense. Morgan states that a
mesh density on the order of 800 triangles per λ_o^2 will produce an error of

Magnitude of e_ϕ (along axis)
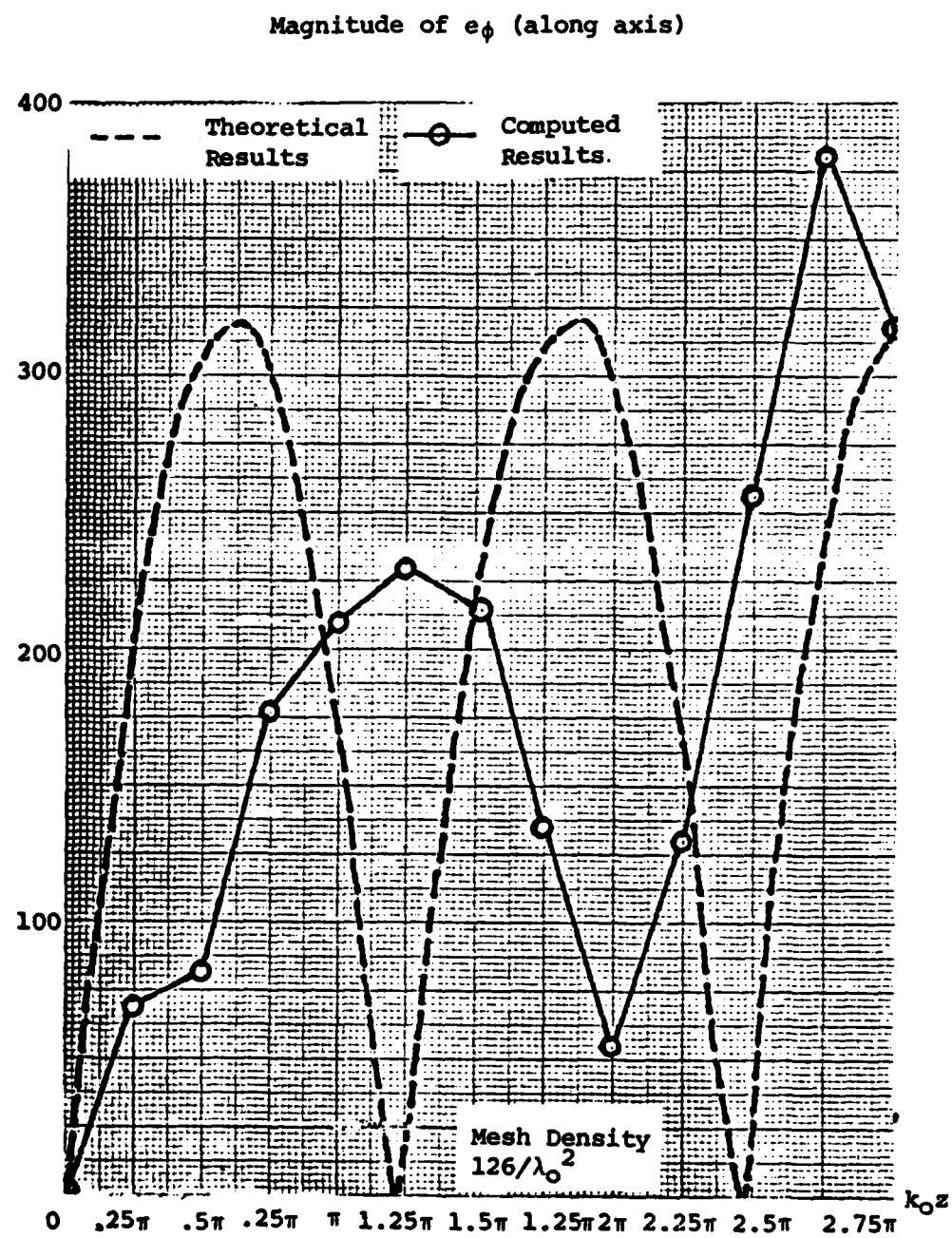
Figure 7. Comparison of Theoretical and Computed Results for Magnitude of e_ϕ; Low Density Mesh

28
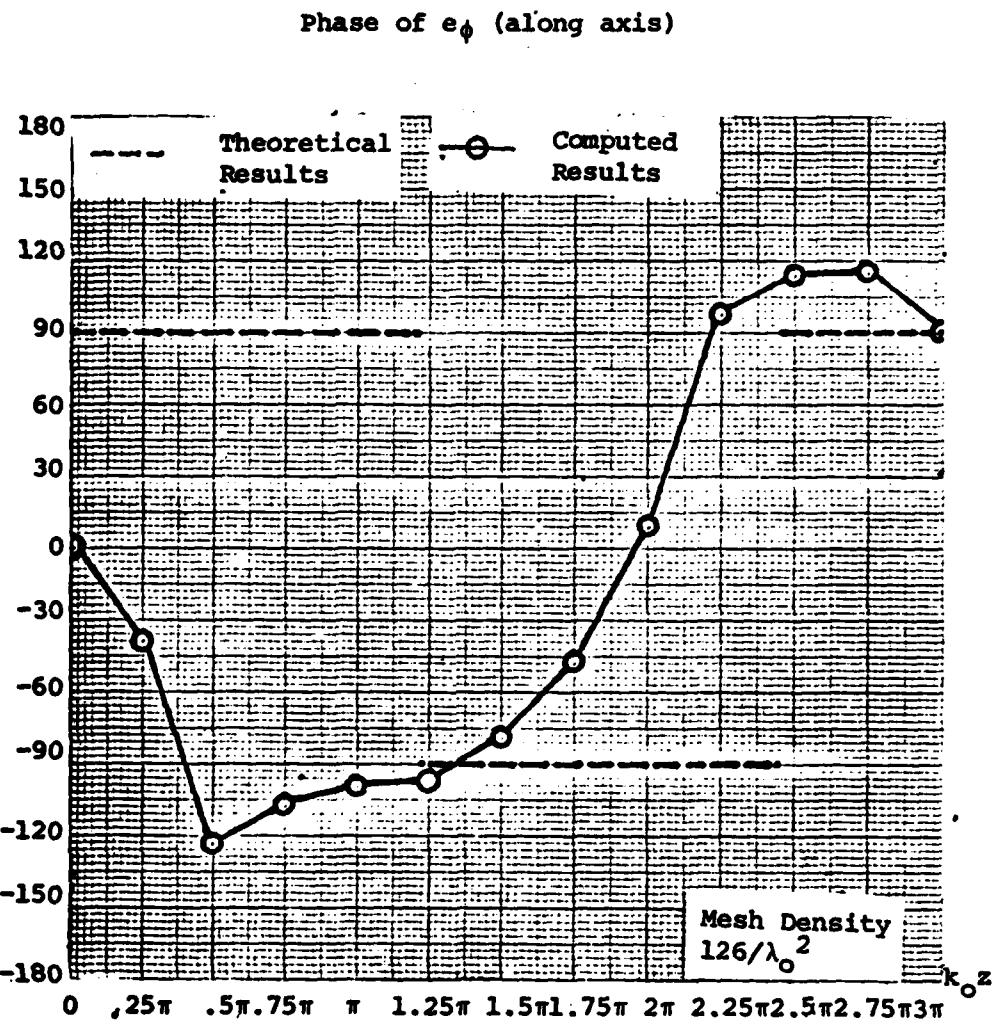
Figure 8. Comparison of Theoretical and Computed Results for Phase of e_ϕ; Low Density Mesh
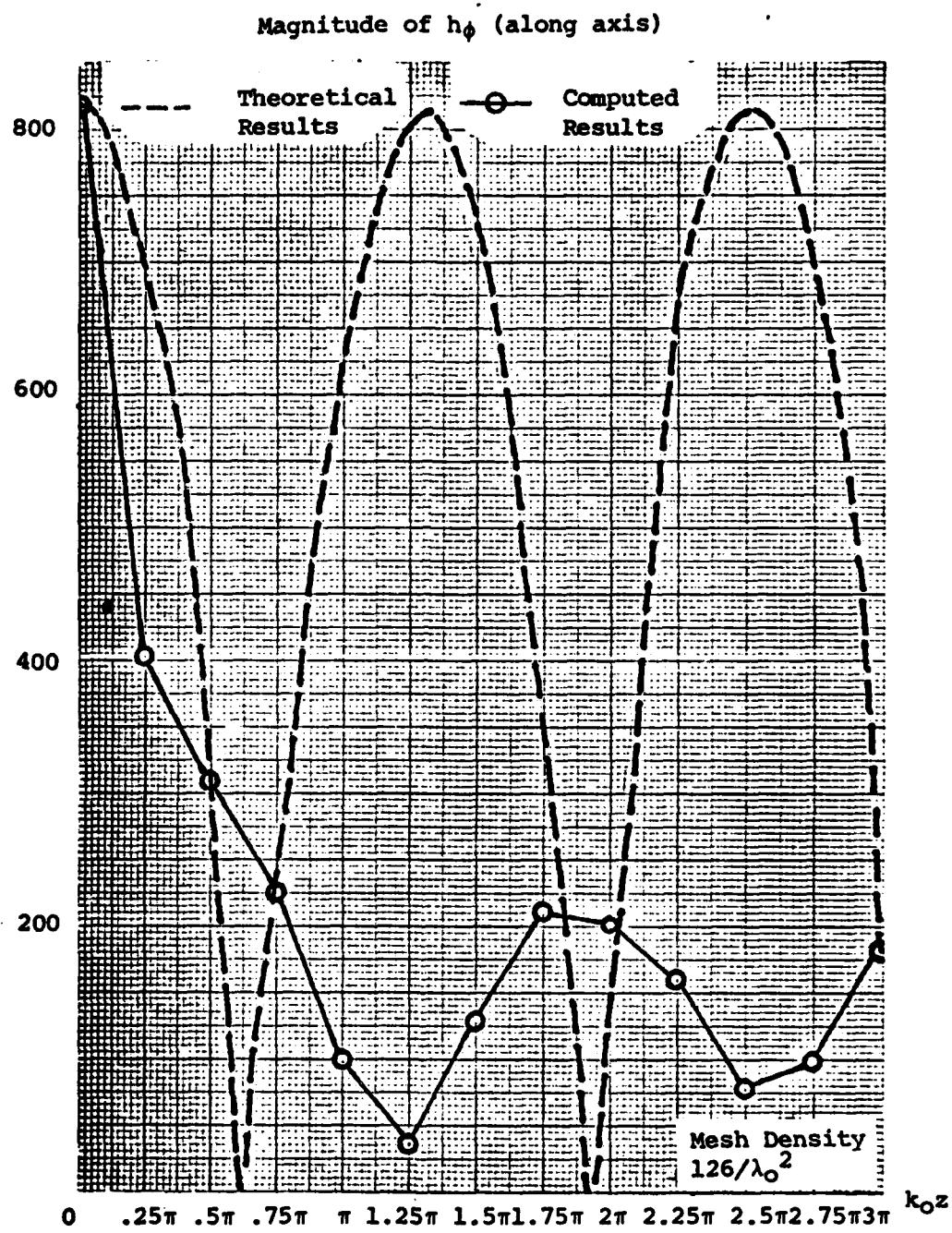
Figure 9. Comparison of Theoretical and Computed Results for Magnitude of h_ϕ; Low Density Mesh

30

Phase of h_ϕ (along axis)
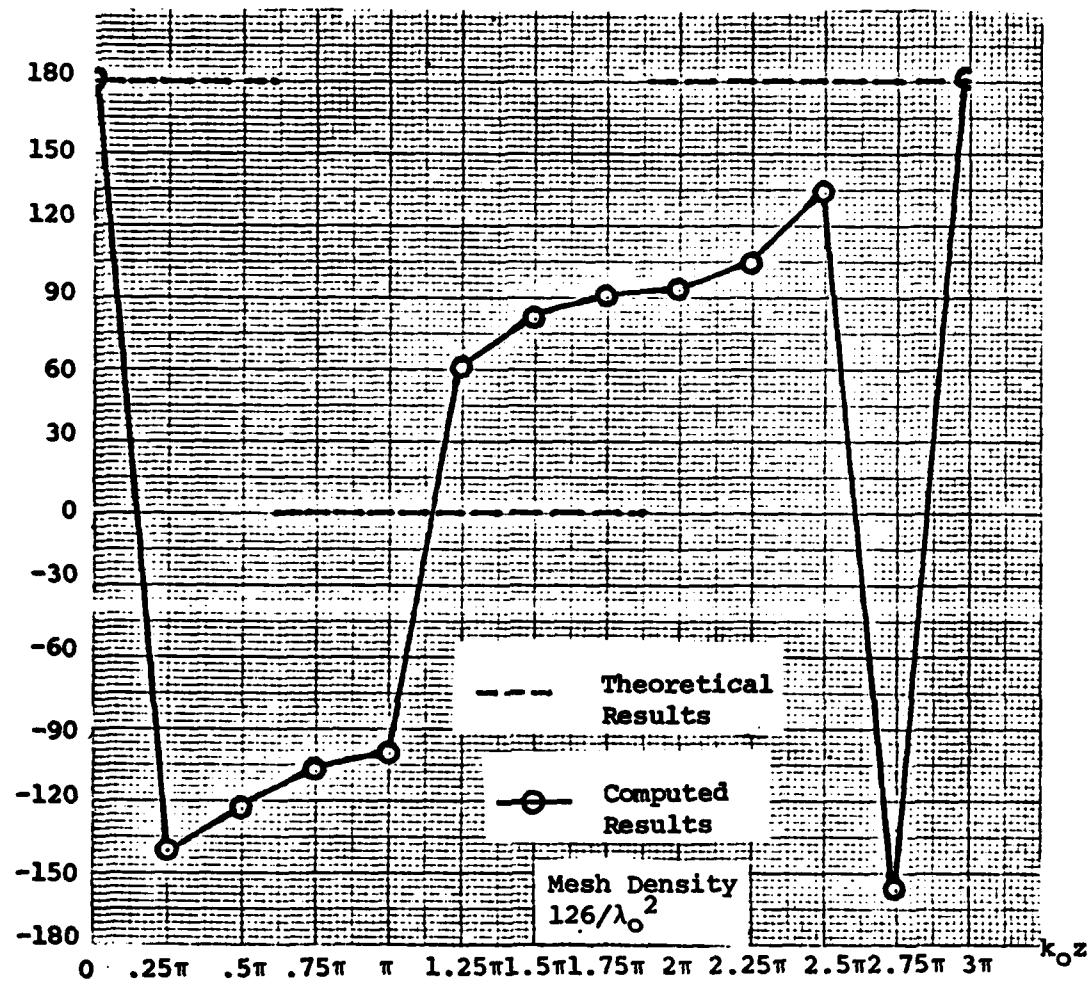
Figure 10. Comparison of Theoretical and Computed Results for Phase of h_ϕ; Low Density Mesh

about 2% (6:209). Consequently, as a second trial case, the mesh
density was increased to this value. The radius of the waveguide section
evaluated was $.3\lambda_o$ with a length of $.4\lambda_o$. On-axis results are presented
in Figures 11, 12, 13 and 14.

In the sense of the error measurement being used, these results
are significantly better than those for the low mesh density. The square
root of the average squared error produced values of .137 for the magni-
tude of e_ϕ and .223 for h_ϕ. In addition, the phases of both e_ϕ and h_ϕ
are very close to the theoretical values.

As a final trial, the length of the waveguide section was decreased
to $.2\lambda_o$ with the same radius as the last case. With 96 triangular ele-
ments, this configuration had a mesh density of $1600/\lambda_o^2$. Figures 15,
16, 17 and 18 contain the results.

Again, in the sense of the error measurement, the results continued
to improve. The average squared error for e_ϕ is .0334 and .108 for h_ϕ.
For both azimuthal fields the phases are very good approximations to the
theoretical results.

Since none of the trials generated a good approximation to the magni-
tude of the standing wave in the interior of the model, the wave equation
for an arbitrary node was evaluated. The interior of the waveguide is
source free in which case the wave equation is

$$\nabla^2 \overline{E} + K^2 \overline{E} = 0 \tag{69}$$

Expanding in terms of e_ϕ and h_ϕ this becomes

$$\frac{1}{R}\frac{\partial}{\partial R}\left(R\frac{\partial e_\phi}{\partial R}\right) - \frac{2e_\phi}{R^2} - \frac{2f_m}{R}\frac{\partial}{\partial R}(R\,e_\phi)$$

$$+ \frac{\partial^2 e_\phi}{\partial Z^2} + e_\phi - 2\,f_m R\,\frac{\partial h_\phi}{\partial Z} = 0 \tag{70}$$

Magnitude of e_ϕ (along axis)
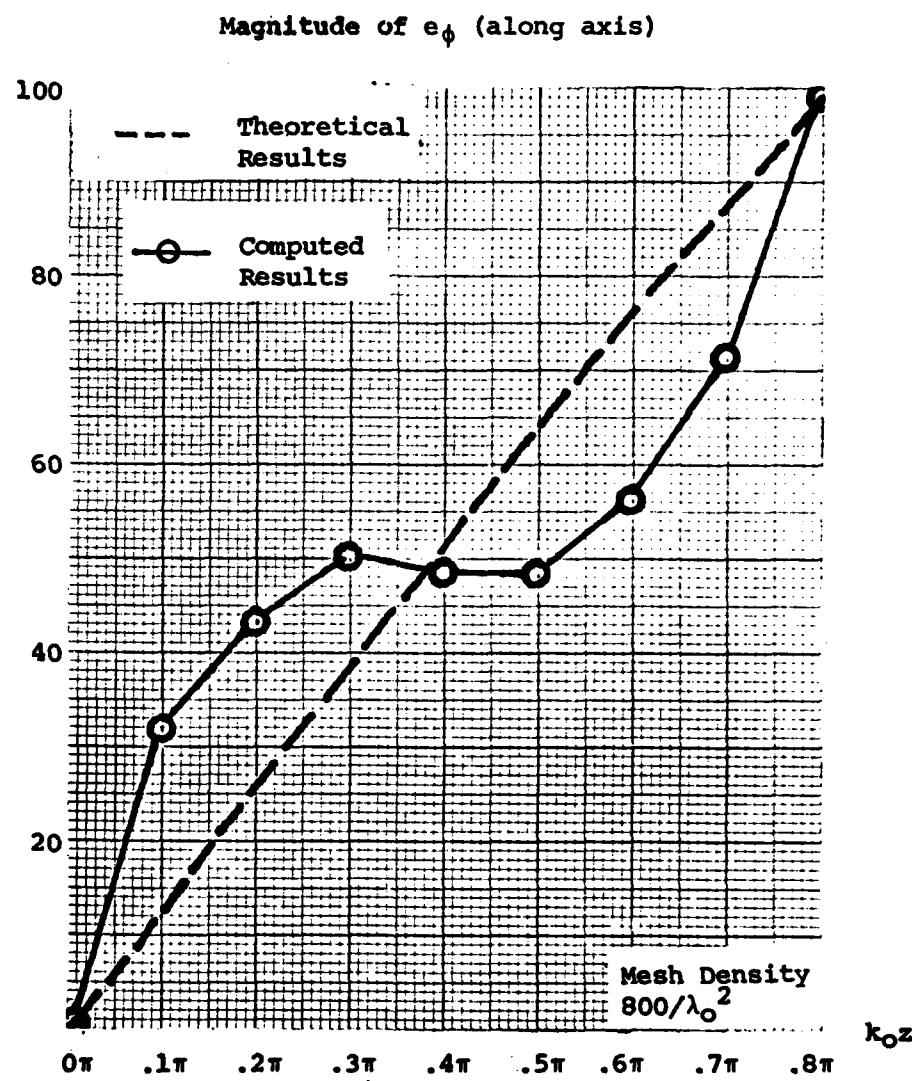
Figure 11. Comparison of Theoretical and Computed
Results for Magnitude of e_ϕ; Medium Density
Mesh

Phase of e_ϕ (along axis)
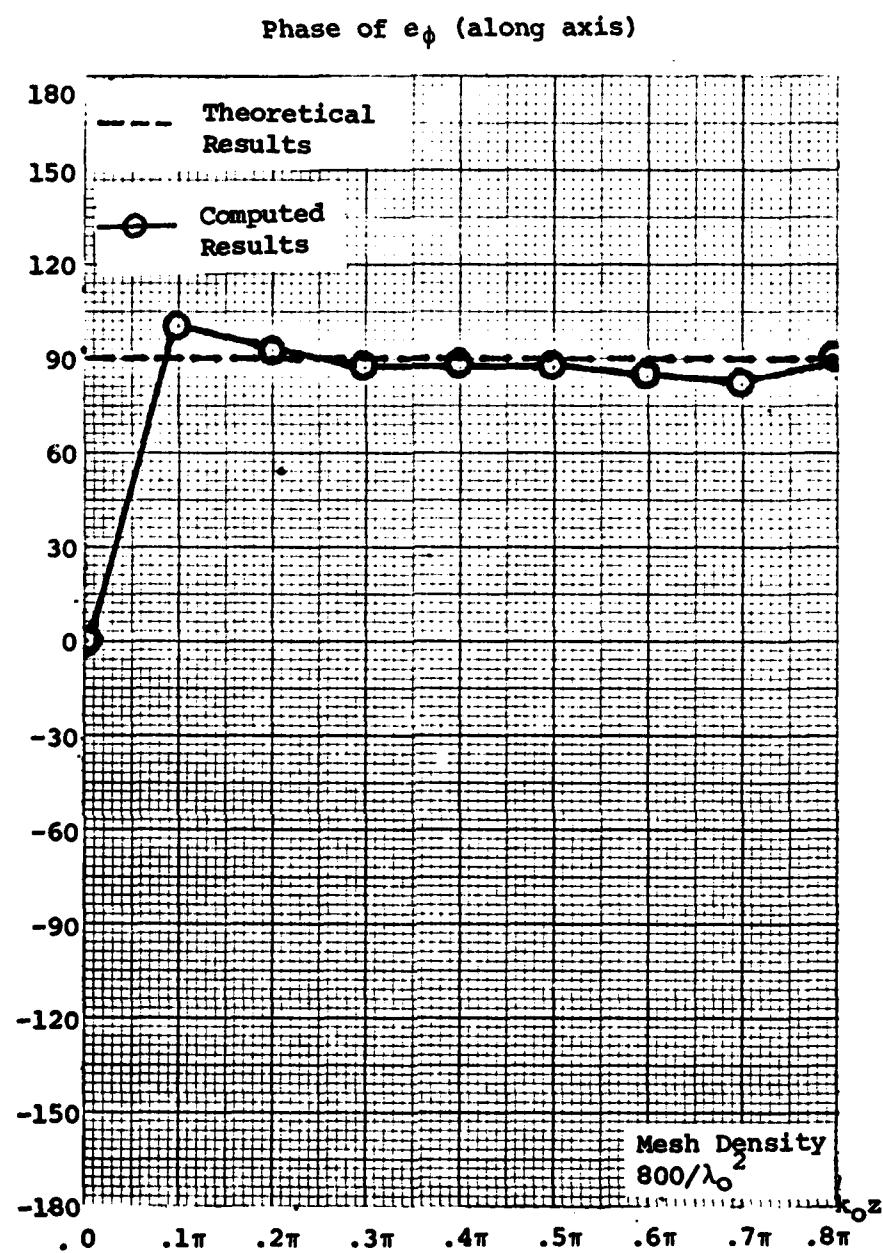
Figure 12. Comparison of Theoretical and Computed Results for Phase of e_ϕ; Medium Density Mesh

Magnitude of h_ϕ (along axis)
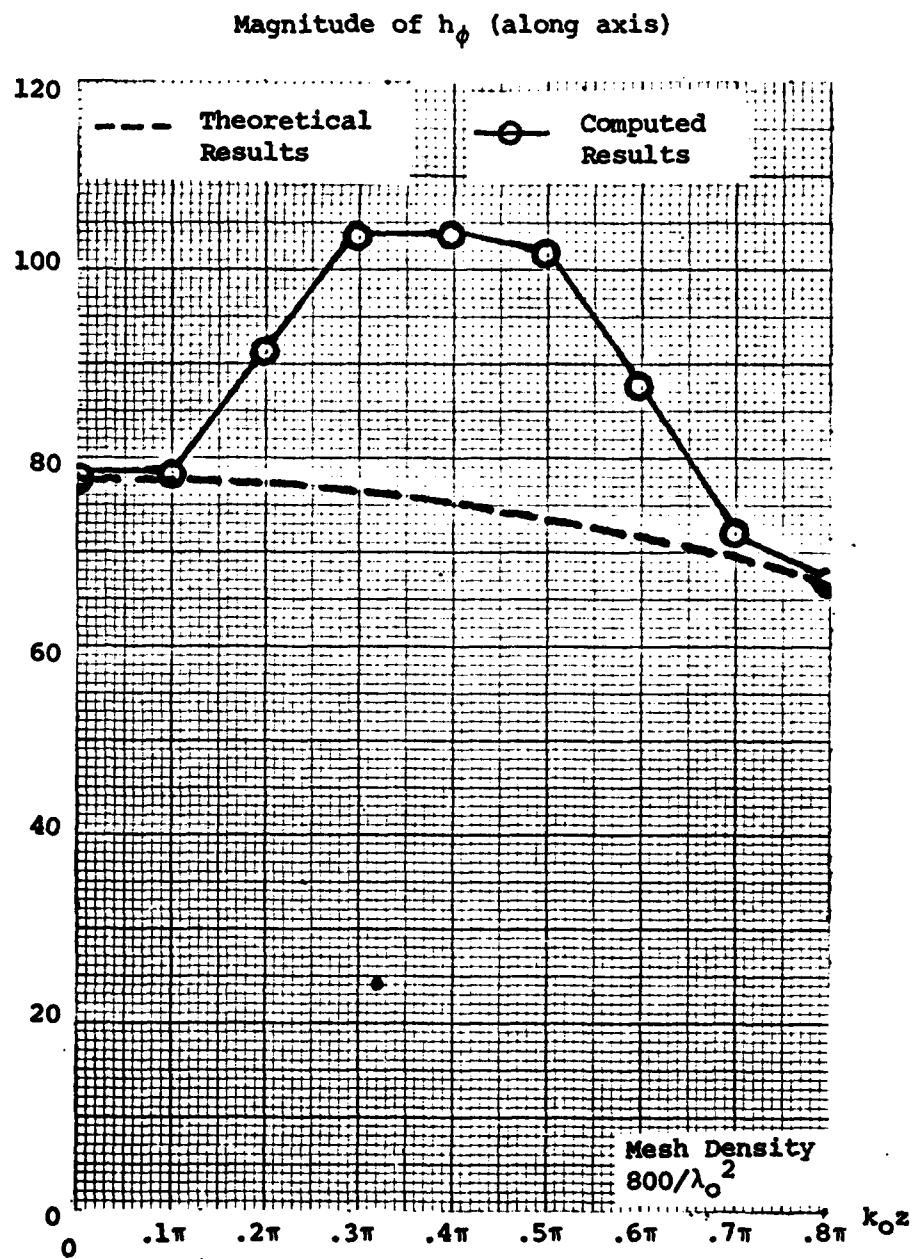
Figure 13. Comparison of Theoretical and Computed Results
for Magnitude of h_ϕ; Medium Density Mesh

Phase of h_ϕ (along axis)
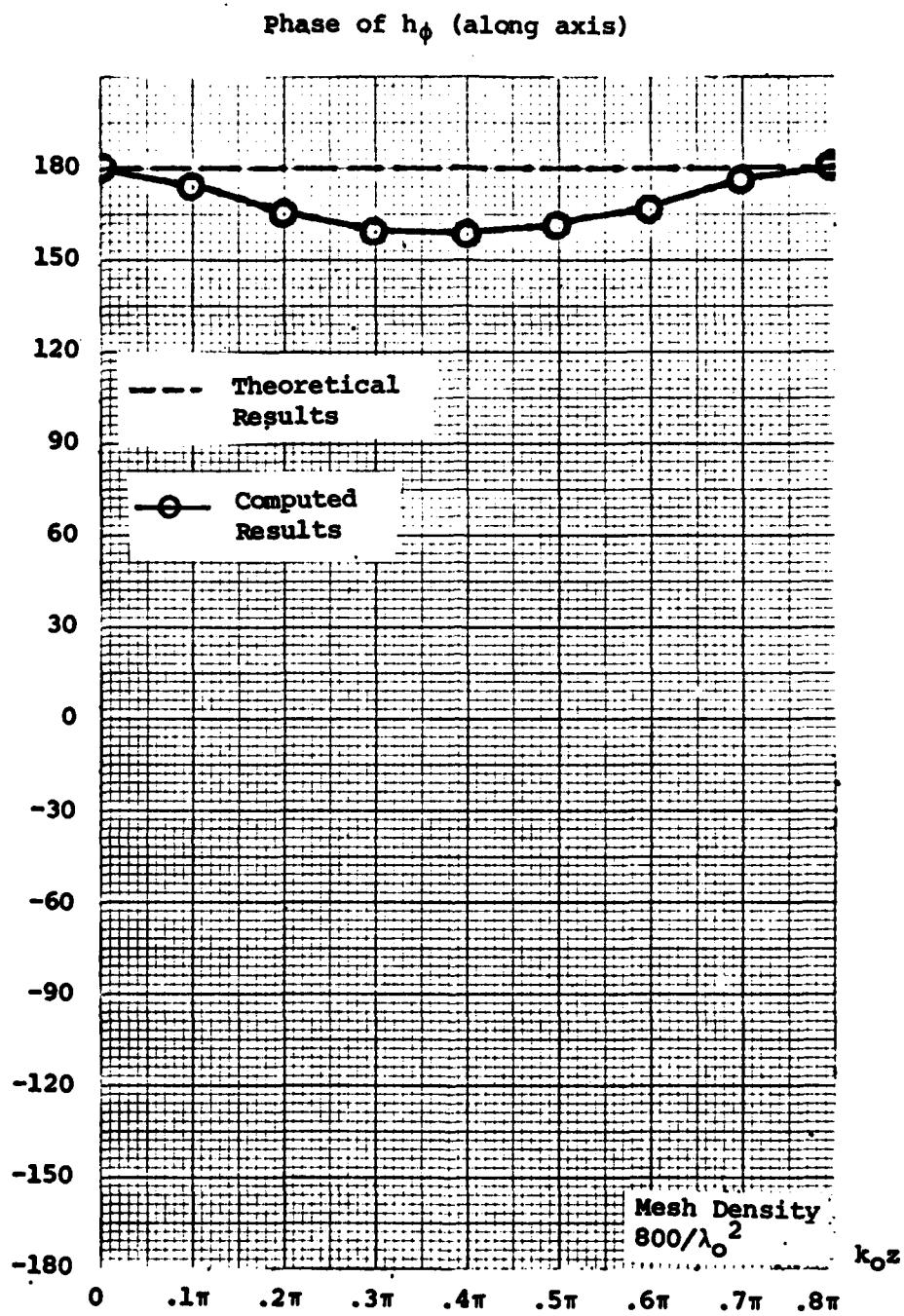
Figure 14. Comparison of Theoretical and Computed Results for Phase of h_ϕ; Medium Density Mesh

36

Magnitude of e_ϕ (along axis)
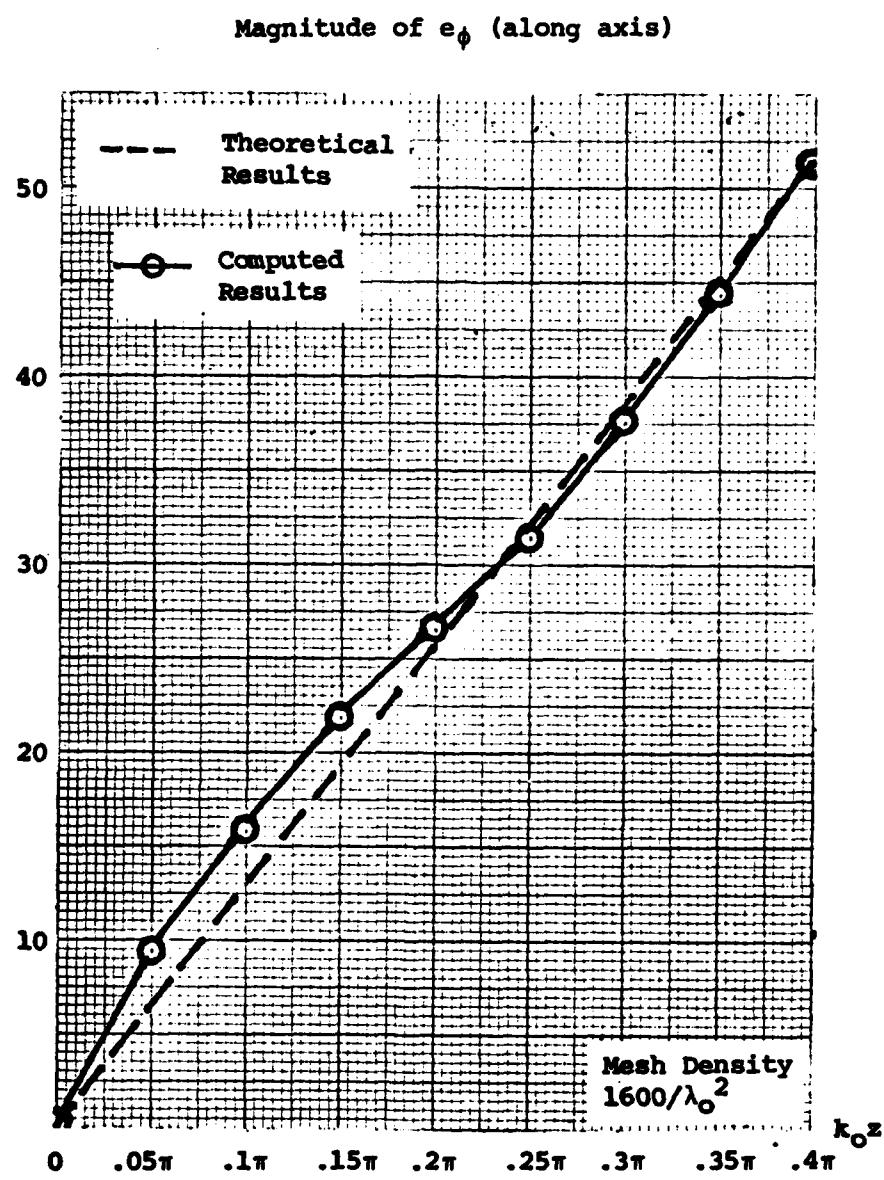
Figure 15. Comparison of Theoretical and Computed Results
for Magnitude of e_ϕ; High Density Mesh

Phase of e_ϕ (along axis)
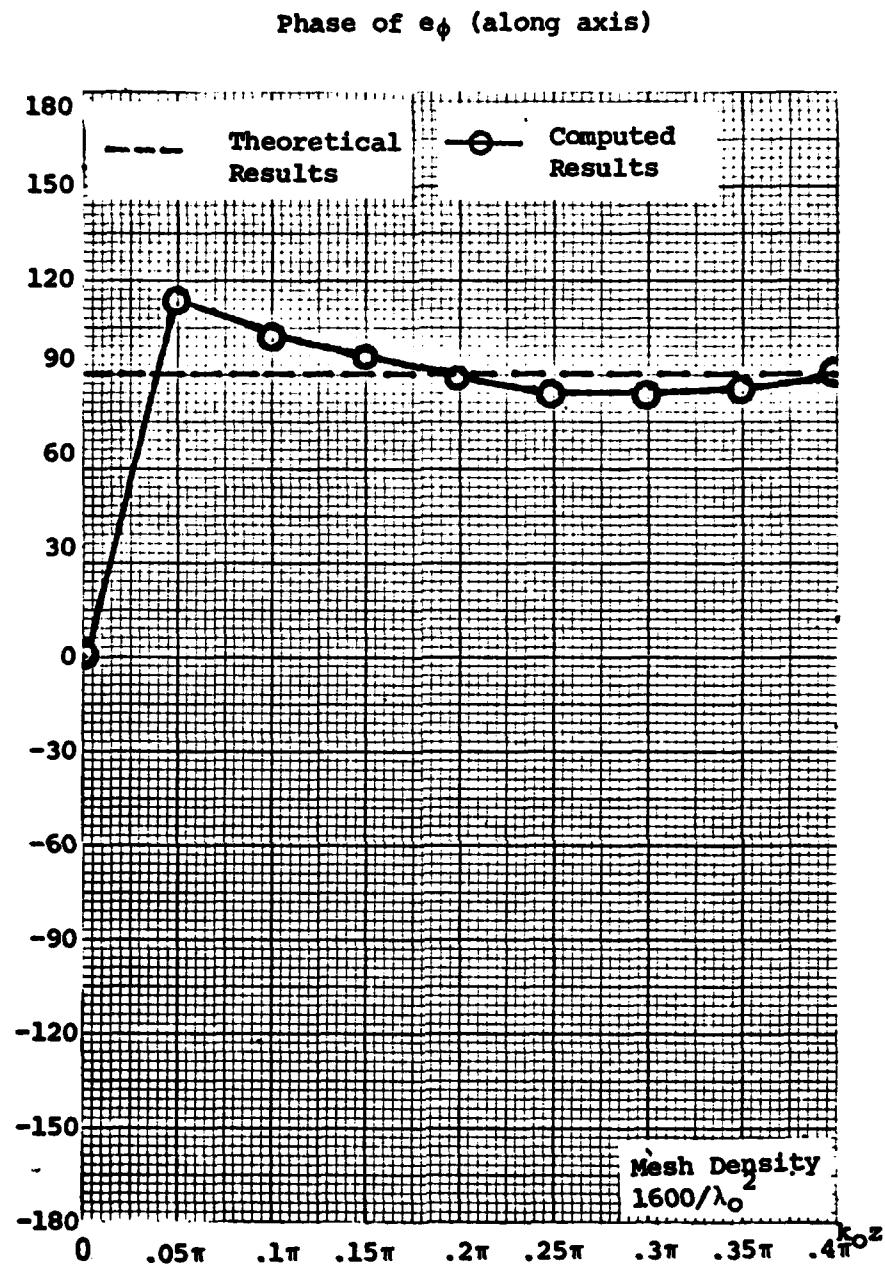
Figure 16. Comparison of Theoretical and Computed Results for Phase of e_ϕ; High Density Mesh

Magnitude of h_ϕ (along axis)
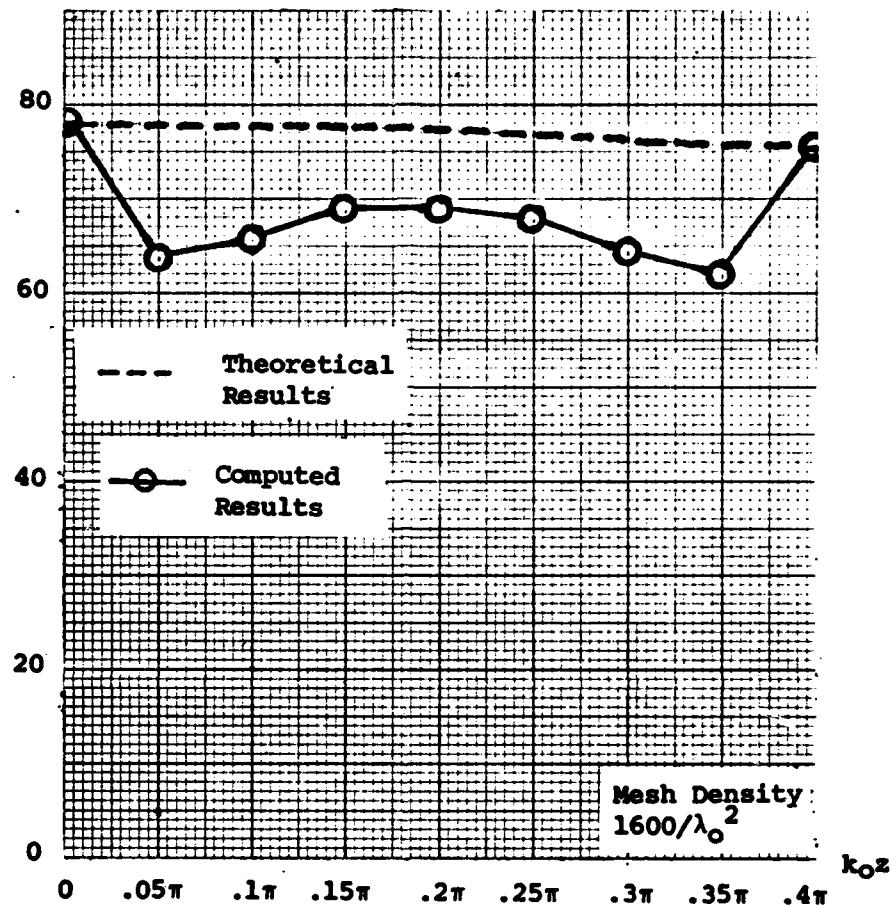
Figure 17. Comparison of Theoretical and Computed Results
for Magnitude of h_ϕ; High Density Mesh
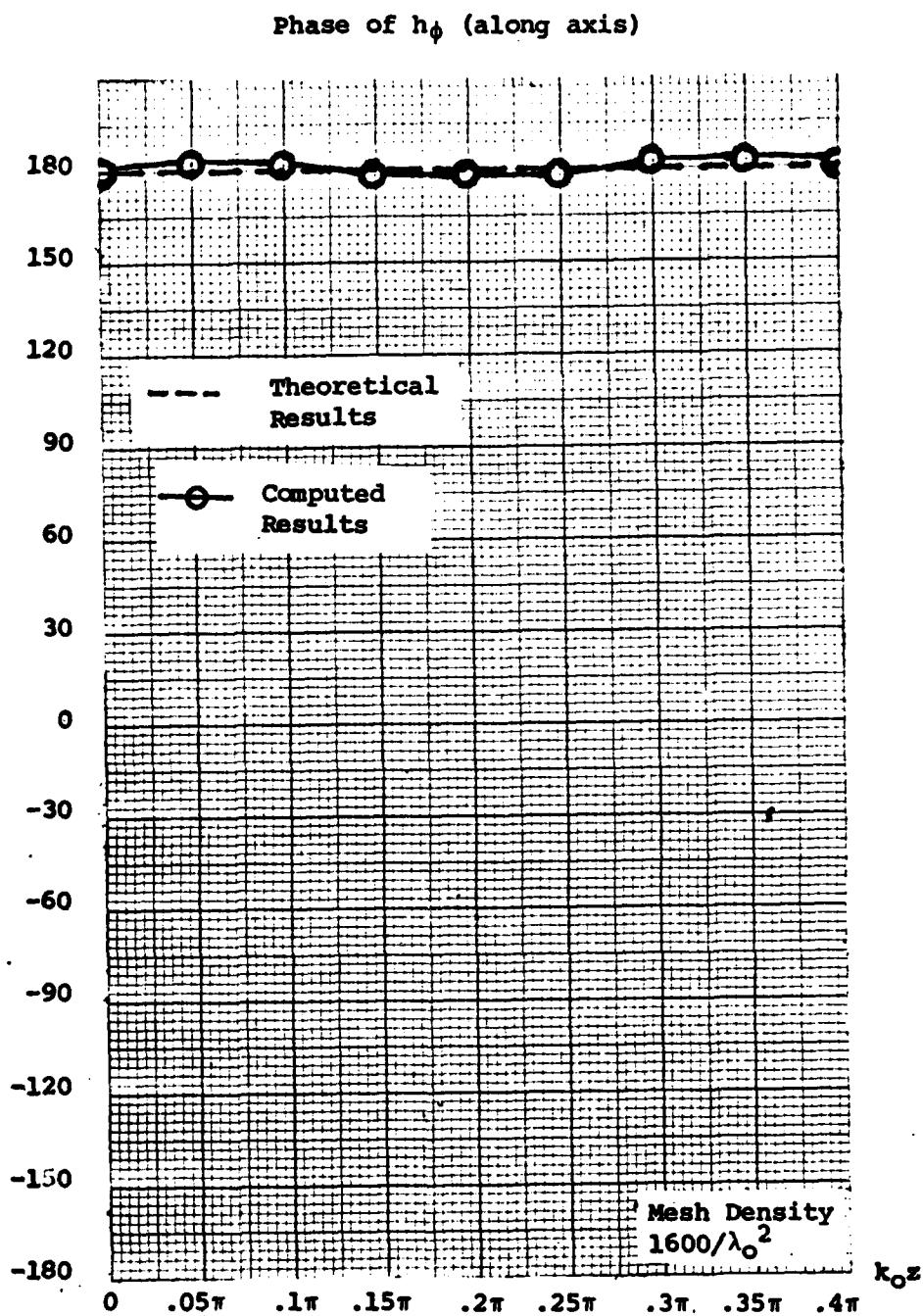
Figure 18. Comparison of Theoretical and Computed Results
for Phase of h_ϕ; High Density Mesh

Since a linear approximation to the fields is being used, the second derivatives do not exist. For this reason, the assumption was made that the fields were smoothly varying and central differences were used to calculate e_ϕ, the results was .1059. This indicates the wave equation is approximately satisfied and the program is functioning properly.

IV. Conclusions and Recommendations

Conclusions

The algorithm used for the finite element implementation of the CAP differential equations functioned properly. For the three mesh densities used, the error measurement indicates the computed results are converging to the theoretical values as the mesh density is increased. A logarithmic plot of these errors is given in Figure 19.
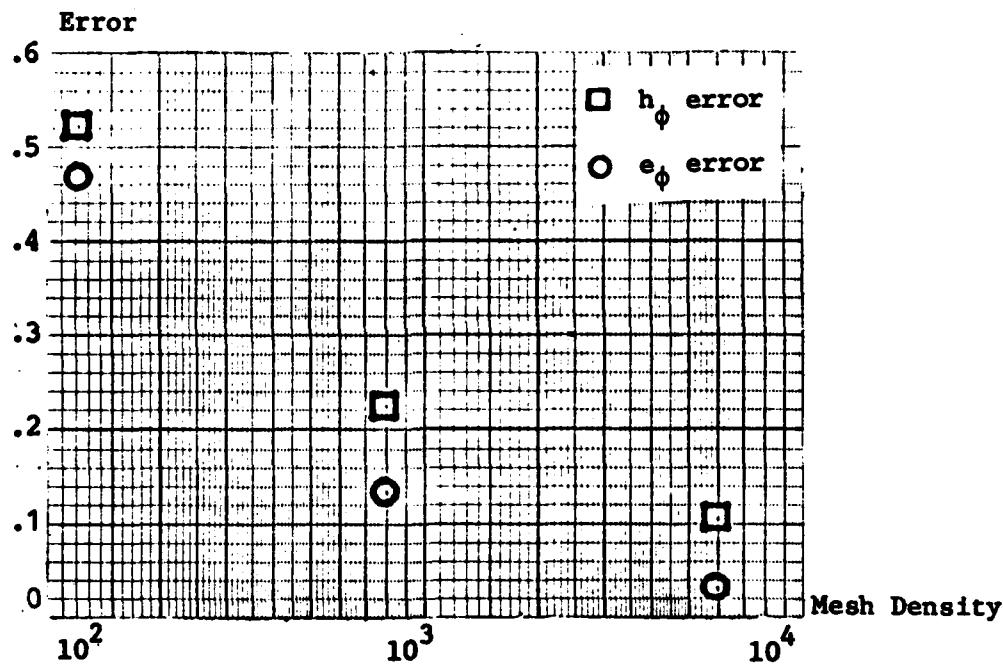
Figure 19.   Plot of the Error Measurement for
Increasing Mesh Densities

This plot indicates that an extraordinarily dense mesh (7500) would be reuqired to achieve acceptable results (2% error). For an inlet model with reasonable dimensions, this mesh requirement is prohibitively large from a computational standpoint.

42

The most likely cause of this problem is the enforcement of Dirichlet boundary conditions for the magnetic field along a conducting surface instead of the Newmann condition. However, the Lagrangian functional for the CAP equations cannot accommodate the Neumann boundary conditions. Therefore the finite element calculation of the coupled azimuthal potentials in the engine inlet model must be abandoned.

Recommendations

The finite difference method could be used to implement the CAP differential equations directly. Additionally, the Neumann boundary conditions for the magnetic field can be enforced quite readily. This numerical method should be investigated extensively as a replacement for the finite element method.

Bibliography

1. Skolnik, Merrill I. Introduction to Radar Systems (Second Edition). New York: McGraw-Hill Book Company, 1980.

2. Moll, John W. and Rolf G. Seecamp. "Calculation of Radar Reflecting Properties of Jet Engine Intakes Using a Waveguide Model," IEEE Transactions on Aerospace and Electronic Systems, AES-6(5): 675-683 (September 1970).

3. Pathak, P. H. and C. C. Huang. "An Analysis of the Electromagnetic Fields Backscattered from a Jet Intake Configuration," Proceedings of the 1980 Radar Camouflage Symposium, sponsored by the USAF Avionics Laboratory and Martin Marietta Corp. (November 1980).

4. Johnson, Thomas W. and D. L. Moffatt. Electromagnetic Scattering by Open Circular Waveguides. PhD dissertation. Ohio State University, December 1980.

5. Morgan, Michael A. et al. "Copuled Azimuthal Potentials for Electromagnetic Field Problems in Inhomogeneous Axially-Symmetric Media," IEEE Transactions on Antennas and Propagation, AP-25(3): 413-417 (May 1977).

6. Morgan, Michael A. and Kenneth K. Mei. "Finite-Element Computation of Scattering by Inhomogenous Penetrable Bodies of Revolution," IEEE Transactions on Antennas and Propagation, AP-27(2): 202-214 (March 1979).

7. Burden, Richard L., J. Douglas Faires and Albert C. Reynolds. Numerical Analysis (Second Edition). Boston: Prindle, Weber and Schmidt, 1981.

8. Huebner, Kenneth H. The Finite Element Method for Engineers. New York: John Wiley and Sons, 1975.

9. Ramo, Simon, John R. Whinnery and Theodor Van Duzer. Fields and Waves in Communication Electronics. New York: John Wiley and Sons, 1965.

10. Hornbeck, Robert W. Numerical Methods. New York: Quantum Publishers, Inc., 1975.

11. Abramowitz, Milton and Irene Stegun. Handbook of Mathematical Functions. U.S. Government Printing Office, Washington, D.C. (1964).

12. Mei, Kenneth K. "Unimoment Method of Solving Antenna and Scattering Problems," IEEE Transactions on Antennas and Propagation, AP-22(6): 760-766 (November 1974).

13. Holand, I. and K. Bell. Finite Element Methods in Stress Analysis. Tredheim, Norway: Tapie, 1969.

Bibliography (contd)

14. Zienkiewicz, O. C. *The Finite Element Method in Engineering Science*. London: McGraw-Hill, 1971.

15. Strang, William G. and George J. Fix. *An Analysis of the Finite Element Method*. Englewood Cliffs, N.J.: Prentice-Hall, 1973.

APPENDIX A

Computer Program

This appendix contains a listing of the computer program used for implementing the finite element method. Definitions of all major variables used in the program are provided.

Variables

RCORD(I) - Real; contains the R coordinate of the Ith node.

ZCORD(I) - Real; contains the Z coordinate of the Ith node.

PLYNML (I,J,K) - Real; contains the K coefficients of the linear polynomial of node J on triangle K.

GAMMAS(I) - Complex; contains the values of the boundary conditions for the azimuthal electric field.

BETAS(I) - Complex; contains the values of the boundary conditions for the azimuthal magnetic field.

GAMNUM(I) - Real; contains the node number of the boundary conditions specified in GAMMAS.

BETNUM(I) - Real; contains the node nubmer of the boundary condition specified in BETAS.

EQUTN1(I,J) - Complex; contains all equations minimized with respect to the electric field nodal values.

EQUTN2(I,J) - Complex; contains all equations minimized with respect to the magnetic field nodal values.

ANSWR(I) - Complex, contains the final computed values of the azimuthal fields.

NUMEL-Integer; the number of elements in the system.

NUMNOD-Integer; the number of nodes in the system.

NODES(I,J) - Integer; contains the node numbers on each triangle.

INTGRL(I) - Real; contains the results of all integrals of the form $R^r Z^s$.

RSLT2(I) - Complex; contains the results of all integrals of the form $\dfrac{R^{I-1}}{R^{2-1}}$.

SYSTEM(I,J) - Complex; contains the system of equations defined in the Lagrangian, before inversion.

46

```
TOM,T30,IO70,CM370000.        T830028,COOPER,4262.
RFL,370000.
ATTACH,TAPE1,CY=001.
ATTACH,TAPE2,CY=001.
ATTACH,IMSL,IMSL,ID=LIBRARY,SN=ASD.
LIBRARY,IMSL.
FTN5(AVSI=T).
REDUCE.
REQUEST,TAPE7,*PF.
LGO,OP=A.
CATALOG,TAPE7,TAPE7,RP=999.
     OVERLAY(XFILE,0,0)
     PROGRAM FINELM
C- THIS PROGRAM WAS WRITTEN BY LT. THOMAS G. COOPER AS PART
C- OF A THESIS PROJECT WHILE A STUDENT AT THE AIR FORCE INSTITUTE
C- OF TECHNOLOGY.  THIS PROGRAM WILL NUMERICALLY SOLVE THE
C- COUPLED AZIMUTHAL POTENTIAL DIFFERENTIAL EQUATIONS BY MEANS
C- OF THE FINITE ELEMENT METHOD.

C- ANSWR MUST BE 1:2NUMNOD; EQUTN1 AND EQUTN2 - NUMNOD X 2NUMNOD
     COMPLEX ANSWR(1:125),EQUTN1(63,125),EQUTN2(63,125)
     COMPLEX GAMMAS(1:50),BETAS(1:50)

C- RCORD AND ZCORD MUST BE 1:NUMNOD; PLYNML - NUMEL X 3 X 3
     REAL RCORD(1:63),ZCORD(1:63),PLYNML(36,3,3)
     REAL BMAG,BANGL,GMAG,GANGL,BESSEL(1:2)
     REAL J11,PI,ARGMT,JPRIME,MMB3J1,MMBSJ8

C- NODES MUST BE NUMEL X 3
```

47

```
      INTEGER NODES(96,3)
      INTEGER GAMNUM(1:50),BETNUM(1:50),GSPEC,BSPEC,INDEX
      INTEGER NUMEL,NUMNOD,IER

      COMMON/OUTDAT/EQUTN1,EQUTN2
      COMMON/POLY/PLYNML
      COMMON/INDATA/RCORD,ZCORD,NODES,NUMEL,NUMNOD
      COMMON/COEFF/ANSWR,GAMMAS,BETAS,GAMNUM,BETNUM,GSPEC,BSPEC

      JII=1.84118
      PI=3.14159
C-- INITIALIZE NUMBER OF SYSTEM NODES AND ELEMENTS
      NUMNOD=63
      NUMEL=96

C-- READ NODE NUMBERS AND COORDINATES
      DO 100 INDEX=1,NUMNOD
      READ(1,*)RCORD(INDEX),ZCORD(INDEX)
100   CONTINUE

C-- READ SYSTEM TOPOLOGY (ELEMENT NUMBERS AND NODE NUMBERS IN
C-- CLOCKWISE FASHION STARTING AT ANY NODE).
      DO 200 INDEX=1,NUMEL
      READ(2,*)NODES(INDEX,1),NODES(INDEX,2),NODES(INDEX,3)
200   CONTINUE

C-- INITIALIZE NUMBER OF SPECIFIED GAMMAS (ELECTRIC FIELD)
C-- AND BETAS (MAGNETIC FIELD).
      GSPEC=21
      BSPEC=21

C-- CLEAR ARRAYS
      DO 250 INDEX=1,50
```

```
          GAMMAS(INDEX)=(0.0,0.0)
          BETAS(INDEX)=(0.0,0.0)
250    CONTINUE

C-  CALCULATE GAMMAS
       GAMNUM(1)=1
       ARGMNT=1.0E-10
       BESSEL(1)=MMBSJ0(ARGMNT,IER)
       BESSEL(2)=MMBSJ1(ARGMNT,IER)
       JPRIME=BESSEL(1)-(1/ARGMNT)*BESSEL(2)
       GAMMAS(1)=CMPLX(0.0,(3.86E2)*JPRIME*SIN((1/(2*PI))*SQRT(
      +(2*PI)**2-(J11/.3)**2)*ZCORD(1)))
       DO 300 INDEX=2,6
          GAMNUM(INDEX)=INDEX
          ARGMNT=J11*RCORD(INDEX)/(PI*.6)
          BESSEL(1)=MMBSJ0(ARGMNT,IER)
          BESSEL(2)=MMBSJ1(ARGMNT,IER)
          JPRIME=BESSEL(1)-(1/ARGMNT)*BESSEL(2)
          GAMMAS(INDEX)=CMPLX(0.0,(3.86E2)*JPRIME*SIN((1/(2*PI))*
      +   SQRT((2*PI)**2-(J11/.3)**2)*ZCORD(INDEX)))
300    CONTINUE
       DO 400 INDEX=7,63,7
          GAMNUM(INDEX/7+6)=INDEX
          GAMMAS(INDEX/7+5)=(0.0,0.0)
400    CONTINUE
       DO 500 INDEX=57,62
          GAMNUM(INDEX-41)=INDEX
          GAMMAS(INDEX-41)=(0.0,0.0)
500    CONTINUE

C-  CALCULATE BETAS
       BETNUM(1)=1
       ARGMNT=J11*1.0E-10
```

```
      BESSEL(2)=MMBSJ1(ARGMNT,IER)
      BETAS(1)=-376.7*((.5)/(J11**2))*((PI*.6)/1.0E-10)*SQRT((2*PI)
     +(J11/.3)**2)*BESSEL(2)*COS((1/(2*PI))*SQRT(
     +(2*PI)**2-(J11/.3)**2)*ZCORD(1))
      DO 600 INDEX=2,6
      BETNUM(INDEX)=INDEX
      ARGMNT=J11*RCORD(INDEX)/(PI*.6)
      BESSEL(2)=MMBSJ1(ARGMNT,IER)
      BETAS(INDEX)=-376.7*((.3)/(J11/.3)**2)*((PI*.5)/RCORD(INDEX))
     +   SQRT((2*PI)**2-(J11/.3)**2)*BESSEL(2)*COS(
     +   (1/(2*PI))*SQRT((2*PI)**2-(J11/.3)**2)*ZCORD(INDEX))
600   CONTINUE
      DO 700 INDEX=7,63,7
      BETNUM(INDEX/7+5)=INDEX
      ARGMNT=J11*RCORD(INDEX)/(PI*.6)
      BESSEL(2)=MMBSJ1(ARGMNT,IER)
      BETAS(INDEX/7+6)=-376.7*((.3)/(J11**2))*((PI*.5)/RCORD(INDEX))
     +   *SQRT((2*PI)**2-(J11/.3)**2)*BESSEL(2)*COS(
     +   (1/(2*PI))*SQRT((2*PI)**2-(J11/.3)**2)*ZCORD(INDEX))
700   CONTINUE
      BETNUM(16)=57
      ARGMNT=J11*1.0E-10
      BESSEL(2)=MMBSJ1(ARGMNT,IER)
      BETAS(16)=-376.7*((.3)/(J11**2))*((PI*.5)/1.0E-10)*SQRT((2*PI
     +(J11/.3)**2)*BESSEL(2)
      DO 800 INDEX=53,62
      BETNUM(INDEX-41)=INDEX
      ARGMNT=J11*RCORD(INDEX)/(PI*.6)
      BESSEL(2)=MMBSJ1(ARGMNT,IER)
      BETAS(INDEX-41)=-376.7*((.3)/(J11**2))*((PI*.5)/RCORD(INDE
     +   SQRT((2*PI)**2-(J11/.3)**2)*BESSEL(2)
800   CONTINUE
C-  PRINT OUT SYSTEM CONFIGURATION DATA.
```

50

```
      WRITE(7,900)NUMNOD,NUMEL
      WRITE(7,1000)
      DO 1100 INDEX=1,NUMNOD
      WRITE(7,1200)INDEX,RCORD(INDEX),ZCORD(INDEX)
 1100 CONTINUE
      WRITE(7,1300)
      DO 1400 INDEX=1,NUMEL
      WRITE(7,1500)INDEX,NODES(INDEX,1),NODES(INDEX,2),NODES(INDEX,3)
 1400 CONTINUE

      CALL OVERLAY('XFILE',1,0)
      CALL OVERLAY('XFILE',2,0)
      CALL OVERLAY('XFILE',3,0)

C- CALCULATE AND DISPLAY MAGNITUDE AND PHASE OF RESULTING GAMMAS
C- AND BETAS.
      WRITE(7,1600)
      DO 1700 INDEX=1,NUMNOD
      IF(REAL(ANSWR(INDEX*2)).EQ.0.0.AND.AIMAG(ANSWR(INDEX*2))
     +    .EQ.0.0) THEN
          BMAG=0.0
          BANGL=0.0
      ELSE
          BMAG=SQRT(REAL(ANSWR(INDEX*2))**2+AIMAG(ANSWR(INDEX*2)))
          BANGL=ATAN2(AIMAG(ANSWR(INDEX*2)),REAL(ANSWR(INDEX*2)))*
     +    180./PI
      END IF
      IF(REAL(ANSWR((INDEX-1)*2+1)).EQ.0.0.AND.AIMAG(ANSWR(
     +    (INDEX-1)*2+1)).EQ.0.0) THEN
          GMAG=0.0
          GANGL=0.0
      ELSE
          GMAG=SQRT(REAL(ANSWR((INDEX-1)*2+1))**2+AIMAG(ANSWR(
```

51

```
+          (INDEX-1)*2+1))**2)
           GANGL=ATAN2(AIMAG(ANSWR((INDEX-1)*2+1)),REAL(ANSWR(
+          (INDEX-1)*2+1)))*180./PI
           END IF
           WRITE(7,1800)INDEX,GMAG,GANGL
           WRITE(7,1800)INDEX,BMAG,BANGL
1700    CONTINUE

        STOP

900     FORMAT(5X,"NO. OF NODES =",I3,"NO. OF ELEMENTS =",I3,//)
1000    FORMAT(5X,"SUMMARY CF NODAL COORDINATES",//,7X,"I",12X,
+       "R(I)",12X,"Z(I)",//)
1200    FORMAT(5X,I3,2(7X,F10.3))
1300    FORMAT(5X,"LISTING OF SYSTEM TOPOLOGY",//,5X,"ELEMENT
+       NUMBER",20X,"NODE NUMBERS",//)
1500    FORMAT(5X,I3,10X,3(5X,I3))
1600    FORMAT(5X,"NODE NUMBERS",10X,"MAGNITUDE",12X,"ANGLE")
1800    FORMAT(5X,I3,10X,2(7X,E10.4))
        END
C-  THIS SUBROUTINE COMPUTES THE AREA OF AN ARBITRARY TRIANGLE.

C-  NODES MUST BE NUMEL X 3
        INTEGER NODES(96,3)
        INTEGER TRANGL,NUMEL,NUMNOD

C-  RCORD AND ZCORD MUST BE 1:NUMNOD
        REAL RCORD(1:63),ZCORD(1:63)
        REAL DEL

        COMMON/INDATA/RCORD,ZCORD,NODES,NUMEL,NUMNOD
```

52

```
      DE_=(.5)*ABS(RCORD(NODES(TRANGL,1))*(ZCORD(NODES(TRANGL,2))
     +-ZCORD(NODES(TRANGL,3)))+RCORD(NODES(TRANGL,2))*
     +(ZCORD(NODES(TRANGL,3))-ZCOFD(NODES(TRANGL,1)))+
     +RCORD(NODES(TRANGL,3))*(ZCORD(NODES(TRANGL,1))-
     +ZCORD(NODES(TRANGL,2))))

      RETURN
      END
      OVERLAY(XFILE,2,0)
      PROGRAM INTGRT
C- THIS SUBROUTINE PERFORMS THE INTEGRATION OF THE LAGRANGIAN
C- FUNCTIONAL OVER ALL ELEMENTS IN THE SYSTEM.  THE EQUATIONS
C- WHICH ARE STATIONARY WITH RESPECT TO THE NODAL COEFFICIENTS
C- OF THE ELECTRIC AND MAGNETIC FIELDS ARE THEN STORED IN TWO
C- SEPARATE MATRICES.

C- EQUTN1 AND EQUTN2 MUST BE NUMNOD X 2AUMNOD
      COMPLEX EQUTN1(63,126),EQUTN2(63,126)
      COMPLEX INTGRL(1:6),RSLT1(1:6),RSLT2(1:6),NULL,IVTRND(1:4)
      COMPLEX ANSWR1,ANSWR2,TEMP1,TEMP2

C- RCORD AND ZCORD MUST BE 1:NUMNOD; PLYXML - NUMEL X 3 X 3
      REAL RCORD(1:63),ZCORD(1:63),PLYXML(96,3,3)
      REAL SLOPE,INTCPT

C- NODES MUST BE NUMEL X 3
      INTEGER NODES(96,3)
      INTEGER INDEX1,INDEX2,INDEX3,INDEX4,INDEX5
      INTEGER INDEX6,INDEX7,NUMEL,NUMNOD,NODCOM(3,2)
      INTEGER ROW,GCOL,BCOL

      COMMON/INDATA/RCORD,ZCORD,NODES,NUMEL,NUMNOD
      COMMON/OUTDAT/EQUTN1,EQUTN2
```

```
      COMMON/POLY/PLYNML

      NULL=(0.0,0.0)

C- INITIALIZE MATRICES
      DO 200 INDEX1=1,NUMNOD
      DO 300 INDEX2=1,2*NUMNOD
      EQUTN1(INDEX1,INDEX2)=NULL
      EQUTN2(INDEX1,INDEX2)=NULL
300   CONTINUE
200   CONTINUE

C- STORE POSSIBLE NODE COMBINATIONS
      NODCOM(1,1)=1
      NODCOM(1,2)=2
      NODCOM(2,1)=2
      NODCOM(2,2)=3
      NODCOM(3,1)=3
      NODCOM(3,2)=1

C- CYCLE FOR ALL TRIANGLES
      DO 400 INDEX1=1,NUMEL

C- PERFORM LINE INTEGRALS
      DO 425 INDX10=1,6
      RSLT1(INDX10)=NULL
425   CONTINUE
      DO 450 INDX11=1,6
      INTGRL(INDX11)=NULL
450   CONTINUE
      DO 500 INDEX2=1,3
      IF(RCCRD(NODES(INDEX1,NODCOM(INDEX2,1))).NE.
     +   RCORD(NODES(INDEX1,NODCOM(INDEX2,2)))) THEN
```

54

```
      SLOPE=(ZCORD(NODES(INDEX1,NODCOM(INDEX2,2)))-
     +ZCORD(NODES(INDEX1,NODCOM(INDEX2,1))))/
     +(RCORD(NODES(INDEX1,NODCOM(INDEX2,2)))-
     +RCORD(NODES(INDEX1,NODCOM(INDEX2,1))))
      INTCPT=-1*SLOPE*RCORD(NODES(INDEX1,NODCOM(INDEX2,1)):
     +ZCORD(NODES(INDEX1,NODCOM(INDEX2,1)))
      INTRMD(1)=CMPLX(RCORD(NODES(INDEX1,NODCOM(INDEX2,
     +2)))**2-RCORD(NODES(INDEX1,NODCOM(INDEX2,1)))**2)
      INTRMD(2)=CMPLX(RCORD(NODES(INDEX1,NODCOM(INDEX2,
     +2)))**3-RCORD(NODES(INDEX1,NODCOM(INDEX2,1)))**3)
      INTRMD(3)=CMPLX(RCORD(NODES(INDEX1,NODCOM(INDEX2,
     +2)))**4-RCORD(NODES(INDEX1,NODCOM(INDEX2,1)))**4)
      INTRMD(4)=CMPLX(RCORD(NODES(INDEX1,NODCOM(INDEX2,
     +2)))**5-RCORD(NODES(INDEX1,NODCOM(INDEX2,1)))**5)
      RSLT1(1)=RSLT1(1)+(1.0/3.0)*SLOPE*INTRMD(2)+
     +(1.0/2.0)*INTCPT*INTRMD(1)
      RSLT1(2)=RSLT1(2)+(1.0/4.0)*SLOPE*INTRMD(3)+
     +(1.0/3.0)*INTCPT*INTRMD(2)
      RSLT1(3)=RSLT1(3)+(1.0/6.0)*(SLOPE**2)*INTRMD(5)+
     +(1.0/3.0)*SLOPE*INTCPT*INTRMD(2)+(1.0/4.0)*
     +(INTCPT**2)*INTRMD(1)
      RSLT1(4)=RSLT1(4)+(1.0/10.0)*(SLOPE**2)*INTRMD(4)+
     +(1.0/4.0)*SLOPE*INTCPT*INTRMD(3)+(1.0/6.0)*
     +(INTCPT**2)*INTRMD(2)
      RSLT1(5)=RSLT1(5)+(1.0/5.0)*SLOPE*INTRMD(4)+
     +(1.0/4.0)*INTCPT*INTRMD(3)
      RSLT1(6)=RSLT1(6)+(1.0/15.0)*(SLOPE**3)*INTRMD(4)+
     +(1.0/4.0)*(SLOPE**2)*INTCPT*INTRMD(3)+
     +(1.0/3.0)*(INTCPT**2)*SLOPE*INTRMD(2)+
     +(1.0/6.0)*(INTCPT**3)*INTRMD(1)
      ANSWR1=CMPLX(ALOG(ABS(RCORD(NODES(INDEX1,
     +NODCOM(INDEX2,2)))-1.0)*(RCORD(NODES(INDEX1,
     +NODCOM(INDEX2,1)))+1.0)/(ABS(RCORD(NODES(INDEX1,
```

```
+          NODCOM(INDEX2,1)))-1.0)*(RCORD(NODES(INDEX1,
+          NODCOM(INDEX2,2)))+1.0)))
+          ANSWR2=CMPLX(ALOG(ABS(RCORD(NODES(INDEX1,
+          NODCOM(INDEX2,2)))-1.0)*(RCORD(NODES(INDEX1,
+          NODCOM(INDEX2,2)))+1.0)/(ABS(RCORD(NODES(INDEX1,
+          NODCOM(INDEX2,1)))-1.0)*(RCORD(NODES(INDEX1,
+          NODCOM(INDEX2,1)))+1.0))))

C-- TEST FOR INTEGRATION PASSING THROUGH SINGULARITY.
          IF(RCORD(NODES(INDEX1,NODCOM(INDEX2,1))).GT.1.0
+          .AND.RCORD(NODES(INDEX1,NODCOM(INDEX2,2)))
+          .LT.1.0) THEN
                RSLT2(1)=.5*(ANSWR1+(0.0,-3.14159265))
                RSLT2(2)=.5*(ANSWR2+(0.0,-3.14159265))
          ELSE IF(RCORD(NODES(INDEX1,NODCOM(INDEX2,1)))
+          .LT.1.0.AND.RCORD(NODES(INDEX1,NODCOM(INDEX2,2)))
+          .GT.1.0) THEN
                RSLT2(1)=.5*(ANSWR1+(0.0,3.14159265))
                RSLT2(2)=.5*(ANSWR2+(0.0,3.14159265))
          ELSE
                RSLT2(1)=.5*ANSWR1
                RSLT2(2)=.5*ANSWR2
          END IF

C-- USE RECURRENCE FORMULA TO GENERATE HIGHER ORDER INTEGRALS.
          DO 600 INDEX3=3,5
                RSLT2(INDEX3)=RSLT2(INDEX3-2)+CMPLX((RCORD(
+          NODES(INDEX1,NODCOM(INDEX2,2)))**(INDEX3-2)-
+          (RCORD(NODES(INDEX1,NODCOM(INDEX2,1)))**
+          (INDEX3-2))/(INDEX3-2))
600       CONTINUE
          INTGRL(1)=INTGRL(1)+SLOPE*RSLT2(3)+INTCPT*RSLT2(2)
          INTGRL(2)=INTGRL(2)+SLOPE*RSLT2(4)+INTCPT*RSLT2(3)
          INTGRL(3)=INTGRL(3)+SLOPE*RSLT2(5)+INTCPT*RSLT2(4)
          INTGRL(4)=INTGRL(4)+(SLOPE**2)*RSLT2(4)+2.*SLOPE*
```

56

```
        INTCPT*RSLT2(3)+(INTCPT**2)*RSLT2(2)
   INTGRL(5)=INTGRL(5)+(SLOPE**3)*RSLT2(5)+3*(SLOPE**2)
  *INTCPT*RSLT2(4)+3*SLOPE*(INTCPT**2)*RSLT2(3)
  +(INTCPT**3)*RSLT2(2)
   INTGRL(6)=INTGRL(6)+(SLOPE**2)*RSLT2(5)+2*SLOPE*
  INTCPT*RSLT2(4)+(INTCPT**2)*RSLT2(3)
        END IF
500   CONTINUE

C- FOR ALL COMBINATIONS OF NODES ON EACH TRIANGLE, PERFORM
C- INTEGRAL SUMMATIONS.
      DO 900 INDEX6=1,3
        DO 950 INDEX7=1,3
          TEMP1=
  PLYNML(INDEX1,INDEX6,1)*PLYNML(INDEX1,INDEX7,1)*
  INTGRL(1)+2*(PLYNML(INDEX1,INDEX6,1)*PLYNML(INDEX1,
  INDEX7,2)+PLYNML(INDEX1,INDEX7,1)*PLYNML(INDEX1,
  INDEX6,2))*INTGRL(2)+(4*PLYNML(INDEX1,INDEX5,2)*
  PLYNML(INDEX1,INDEX7,2)+PLYNML(INDEX1,INDEX5,3)+
  PLYNML(INDEX1,INDEX7,3))*INTGRL(3)+.5*(PLYNML(
  INDEX1,INDEX6,1)*PLYNML(INDEX1,INDEX7,3)+PLYNML(
  INDEX1,INDEX7,1)*PLYNML(INDEX1,INDEX5,3))*INTGRL(4)+
  (1.0/3.0)*(PLYNML(INDEX1,INDEX6,3)*PLYNM_(INDEX5,2)+
  INDEX7,3))*INTGRL(5)+(PLYNML(INDEX1,INDFX(INDEX7,2)+
  PLYNML(INDEX1,INDEX7,3)*PLYNML(INDEX6,3))*INTGRL(6)
  PLYNML(INDEX1,INDEX6,3)*INTGRL(6)

C- CONTINUE TO SUM THE INTEGRALS IN THE SAME MANNER.
          TEMP1=TEMP1-
  PLYNML(INDEX1,INDEX6,1)*PLYNML(INDEX1,INDEX7,1)*
  RSLT1(1)-(PLYNML(INDEX1,INDEX6,1)*PLYNM_(
  INDEX1,INDEX7,2)+PLYNML(INDEX1,INDEX7,1)*
  PLYNML(INDEX1,INDEX6,2))*RSLT1(2)-(PLYNM_(
  INDEX1,INDEX6,1)*PLYNML(INDEX1,INDEX7,3)+
```

```
        PLYNML(INDEX1,INDEX7,1)+PLYNML(INDEX1,INDEX6,
     +  3))*RSLT1(3)-(PLYNML(INDEX1,INDEX5,3)*PLYNML(
     +  INDEX1,INDEX7,2)+PLYNML(INDEX1,INDEX7,3)*
     +  PLYNML(INDEX1,INDEX6,2))*RSLT1(4)-PLYNML(
     +  INDEX1,INDEX6,2)*PLYNML(INDEX1,INDEX7,2)+
     +  RSLT1(5)-PLYNML(INDEX1,INDEX6,3)*PLYNML(
     +  INDEX1,INDEX7,3)*RSLT1(6)
        TEMP2=
     +  (PLYNML(INDEX1,INDEX6,1)*PLYNML(INDEX1,INDEX7,3)-
     +  PLYNML(INDEX1,INDEX7,1)*PLYNML(INDEX1,INDEX5,3))*
     +  INTGRL(1)+2*(PLYNML(INDEX1,INDEX6,2)+PLYNML(INDEX1,
     +  INDEX7,3)-PLYNML(INDEX1,INDEX7,2)*PLYNM_(INDEX1,
     +  INDEX6,3))*INTGRL(2)
        ROW=NODES(INDEX1,INDEX6)
        GCOL=(NODES(INDEX1,INDEX7)-1)*2+1
        BCOL=(NODES(INDEX1,INDEX7))*2
        EQUTN1(ROW,GCOL)=EQUTN1(ROW,GCOL)+TEMP1
        EQUTN1(ROW,BCOL)=EQUTN1(ROW,BCOL)+TEMP2
        EQUTN2(ROW,BCOL)=EQUTN2(ROW,BCOL)+TEMP1
        EQUTN2(ROW,GCOL)=EQUTN2(ROW,GCOL)-TEMP2
950     CONTINUE
900     CONTINUE
400     CONTINUE
        RETURN
        END
        OVERLAY(XFILE,1,0)
        PROGRAM PLYCLC
C- THIS SUBROUTINE CALCULATES A LINEAR POLYNOMIAL FOR EACH NODE
C- ON EVERY TRIANGLE. THIS POLYNOMIAL HAS A VALUE OF ONE AT A
C- SINGLE NODE AND IS ZERO AT THE OTHER NODES ON THE TRIANGLE.

C- NODES MUST BE NUMEL X 3
        INTEGER NODES(96,3)
```

58

```fortran
      INTEGER NUMEL,INDEX1(1:3),INDEX2(1:3),NUMNOD

C-- RCORD AND ZCORD MUST BE 1:NUMNOD: PLYNML - NUMEL X 3 X 3
      REAL RCORD(1:63),ZCORD(1:63),PLYNML(?6,3,3)
      REAL DEL

      COMMON/POLY/PLYNML
      COMMON/INDATA/RCORD,ZCORD,NODES,NUMEL,NUMNOD

C-- DEVELOP A LOOK UP TABLE FOR INDEXING PURPOSES.
      INDEX1(1)=2
      INDEX1(2)=3
      INDEX1(3)=1
      INDEX2(1)=3
      INDEX2(2)=1
      INDEX2(3)=2

C-- CYCLE FOR EACH TRIANGLE
      DO 100 I=1,NUMEL
      CALL AREA(I,DEL)
C-- CYCLE FOR EACH MODE
      DO 200 J=1,3
      PLYNML(I,J,1)=(RCORD(NODES(I,INDEX1(J)))*ZCORD(NODES(I,INDEX2(J)))-
     +     ZCORD(NODES(I,INDEX1(J)))-
     +     RCORD(NODES(I,INDEX1(J)))*
     +     ZCORD(NODES(I,INDEX2(J))))/(2*DEL)
      PLYNML(I,J,2)=(ZCORD(NODE (I,INDEX2(J)))-
     +     ZCORD(NODES(I,INDEX1(J))))/(2*DEL)
      PLYNML(I,J,3)=(RCORD(NODES(I,INDEX1(J)))-
     +     RCORD(NODES(I,INDEX2(J))))/(2*DEL)
200   CONTINUE
100   CONTINUE
      RETURN
```

59

```
      END
      OVERLAY(XFILE,3,0)
      PROGRAM SOLVER
C- THIS SUBROUTINE ASSEMBLES ALL THE INTEGRAL EQUATIONS INTO
C- A LINEAR SYSTEM.  BOUNDARY CONDITIONS ARE THEN ENFORCED IN
C- THE SYSTEM AND THE ENTIRE SYSTEM IS THE SIMULTANEOUSLY
C- SOLVED.
C
C- SYSTEM MUST BE 2NUMNOD X 2NUMNOD; ANSWR - 1:2NUMNOD;
C- WA - 1:2NUMNOD(2NUMNOD+2); WK - 1:2NUMNOD; EQUTN1 - NUMNOD X
C- 2NUMNOD   EQUTN2 - NUMNOD X 2NUMNOD
      COMPLEX SYSTEM(126,126),ANSWR(1:126)
      COMPLEX EQUTN1(63,126),EQUTN2(63,126)
      COMPLEX WA(1:16126),WK(1:126)
      COMPLEX GAMMAS(1:50),BETAS(1:50)
C
C- RCORD AND ZCORD MUST BE 1:NUMNOD
      REAL RCORD(1:63),ZCORD(1:63)
C
C- NODES MUST BE NUMEL X 3
      INTEGER NODES(96,3)
      INTEGER NUMEL,NUMNOD,GAMNUM(1:50),BETNUM(1:50),GSPEC,BSPEC
      INTEGER IER,INDEX1,INDEX2

      COMMON/CCEFF/ANSWR,GAMMAS,BETAS,GAMNUM,BETNUM,GSPEC,BSPEC
      COMMON/OUTDAT/EQUTN1,EQUTN2
      COMMON/INDATA/RCORD,ZCORD,NODES,NUMEL,NUMNOD
C
C- CLEAR ARRAYS
      DO 100 INDEX1=1,2*NUMNOD
      ANSWR(INDEX1)=(0.0,0.0)
      DO 200 INDEX2=1,2*NUMNOD
      SYSTEM(INDEX1,INDEX2)=(0.0,0.0)
```

60

```
200     CONTINUE
100   CONTINUE

C-- ASSEMBLE THE EQUATIONS
      DO 300 INDEX1=1,NUMNOD
        DO 400 INDEX2=1,2*NUMNOD
          SYSTEM((INDEX1-1)*2+1,INDEX2)=EQUTN1(INDEX1,INDEX2)
          SYSTEM(INDEX1*2,INDEX2)=EQUTN2(INDEX1,INDEX2)
400     CONTINUE
300   CONTINUE

C-- ENFORCE GAMMA BOUNDARY CONDITIONS
      DO 500 INDEX1=1,GSPEC
        DO 600 INDEX2=1,2*NUMNOD
          SYSTEM((GAMNUM(INDEX1)-1)*2+1,INDEX2)=(0.0,0.0)
600     CONTINUE
        DO 700 INDEX3=1,2*NUMNOD
          ANSWR(INDEX3)=ANSWR(INDEX3)-GAMMAC(INDEX1)*
     +    SYSTEM(INDEX3,(GAMNUM(INDEX1)-1)*2+1)
          SYSTEM(INDEX3,(GAMNUM(INDEX1)-1)*2+1)=(0.0,0.0)
700     CONTINUE
        SYSTEM((GAMNUM(INDEX1)-1)*2+1,(GAMNUM(INDEX1)-1)*2+1)=
     +    (1.0,0.0)
        ANSWR((GAMNUM(INDEX1)-1)*2+1)=GAMMAS(INDEX1)
500   CONTINUE
C-- ENFORCE BETA BOUNDARY CONDITIONS
      DO 800 INDEX1=1,BSPEC
        DO 900 INDEX2=1,2*NUMNOD
          SYSTEM(BETNUM(INDEX1)*2,INDEX2)=(0.0,0.0)
900     CONTINUE
        DO 1000 INDEX3=1,2*NUMNOD
          ANSWR(INDEX3)=ANSWR(INDEX3)-BETAC(INDEX1)*
     +    SYSTEM(INDEX3,BETNUM(INDEX1)*2)
```

61

```fortran
          SYSTEM(INDEX3,BETNUM(INDEX1)*2)=(0.0,0.0)
1000      CONTINUE
          SYSTEM(BETNUM(INDEX1)*2,BETNUM(INDEX1)*2)=(1.0,0.0)
          ANSWR(BETNUM(INDEX1)*2)=BETAS(INDEX1)
800       CONTINUE
C-  SOLVE THE EQUATIONS
          CALL LEQ2C(SYSTEM,2*NUMMOD,2*NUMMOD,ANSWR,1,2*NUMMOD,0,WA,WK,

C-  WRITE OUT ERROR CODE
          WRITE(7,725)IER
725       FORMAT(5X,'IER =',I3)

          RETURN
          END
```

VITA

Thomas Gerard Cooper was born on 30 december 1955 in Port Huron, Michigan. He graduated from high school in Bad Axe, Michigan in 1974 and attended the U.S. Air Force Academy from which he received the degree Bachelor of Science in Electrical Engineering. Upon graduation he was assigned to the Air Force Avionics Laboratory and worked in the Digital Signal Processing group until entering the School of Engineering, Air Force Institute of Technology, in June 1981.

Permanent address: 1048 West Northwood Drive
Caro, Michigan 48723

REPORT DOCUMENTATION PAGE	READ INSTRUCTIONS BEFORE COMPLETING FORM

1. REPORT NUMBER	2. GOVT ACCESSION NO.	3. RECIPIENT'S CATALOG NUMBER
AFIT/GE/EE/82D-25	A124 684	

4. TITLE (and Subtitle)	5. TYPE OF REPORT & PERIOD COVERED
A FINITE ELEMENT COMPUTATION OF THE ELECTROMAGNETIC FIELDS IN AN ENGINE INLET MODEL	MS Thesis
	6. PERFORMING ORG. REPORT NUMBER

7. AUTHOR(s)	8. CONTRACT OR GRANT NUMBER(s)
Thomas G. Cooper, 1Lt	

9. PERFORMING ORGANIZATION NAME AND ADDRESS	10. PROGRAM ELEMENT, PROJECT, TASK AREA & WORK UNIT NUMBERS
Air Force Institute of Technology (AFIT-EN) Wright-Patterson AFB, Ohio 45433	

11. CONTROLLING OFFICE NAME AND ADDRESS	12. REPORT DATE
	December, 1982
	13. NUMBER OF PAGES
	64

14. MONITORING AGENCY NAME & ADDRESS(if different from Controlling Office)	15. SECURITY CLASS. (of this report)
	Unclassified
	15a. DECLASSIFICATION/DOWNGRADING SCHEDULE

16. DISTRIBUTION STATEMENT (of this Report)

Approved for public release; distribution unlimited

17. DISTRIBUTION STATEMENT (of the abstract entered in Block 20, if different from Report)

18. SUPPLEMENTARY NOTES

Approved for public release; IAW AFR 190-17
Approved for public release: IAW AFR 190-17

LYNN E. WOLAVER
Dean for Research and Professional Development
Air Force Institute of Technology (ATC)
Wright-Patterson AFB OH 45433

4 JAN 1983

19. KEY WORDS (Continue on reverse side if necessary and identify by block number)

Finite Element Method
Coupled Azimuthal Potentials
Electromagnetic Scattering
Engine Inlet

20. ABSTRACT (Continue on reverse side if necessary and identify by block number)

The method of coupled azimuthal potentials (CAP) was applied to a waveguide model of an axially symmetric engine inlet to analyze the fields in the region where the front face of the engine terminates the waveguide. Appropriate boundary conditions were derived and the finite element method was used to solve for the potentials.

The Lagrangian of the CAP equations does not provide for the enforcement of Neumann boundary conditions. This prevents exact implementation of the correct boundary conditions for the azimuthal magnetic field.

DD FORM 1473 1 JAN 73   EDITION OF 1 NOV 65 IS OBSOLETE

Dirichlet boundary conditions for the azimuthal electric and magnetic fields were enforced for a standing wave condition in the inlet model with a conducting back plate termination. The computed values for the interior field components were compared with the theoretical values by evaluating the standard deviation. Three trials were performed with varying finite element mesh densities. It was found that as the mesh density increased, the standard deviation for the computed field components decreased. However, from an interpolation of the error measurements, it was determined that an extremely fine mesh is required for an acceptable error (approximately 7500 tringles/ λ_o^2 for 2% error). For this reason the finite element implementation of the CAP equations for this jet engine inlet model is unfeasible.